Physics – Uspekhi **47** (6) 555 – 582 (2004)

REVIEWS OF TOPICAL PROBLEMS PACS numbers: 41.20.Jb, 52.35.Hr, 52.55.Hc

Electromagnetic waves in a magnetized plasma near the critical surface

A V Timofeev

DOI: 10.1070/PU2004v047n06ABEH001714

Contents

Abstract. Electromagnetic waves in a plasma in a magnetic field give rise to enhanced refraction, produce a change in polarization, and cause electromagnetic energy to flow from one wave mode to another when propagating near the critical surface (CS), the one where the electron Langmuir frequency is equal to the wave frequency. A simple unified model of all phenomena taking place near the CS is proposed. These phenomena are due to electromagnetic waves linearly interacting with electron Langmuir oscillations which are localized at the CS in a cold plasma. This interaction manifests itself most strikingly in electron Langmuir oscillation energy escaping directly into a vacuum in the form of electromagnetic radiation.

1. Introduction

It is well known that electromagnetic waves cannot propagate in a plasma whose density exceeds a critical value deduced from the condition of equality of the electron plasma frequency ω_{pe} to the oscillation frequency ω. In the case of an inhomogeneous plasma, the surface on which this condition is fulfilled is referred to as the critical surface (CS). The presence of a magnetic field makes it possible for the waves to penetrate behind the CS. However, the penetration is accompanied by complicated physical processes in the vicinity of the CS. Specifically, the waves experience enhanced refraction, change their polarization, and undergo reflection and transformation to oscillations of a different type.

These processes began to attract the interest of researchers over 50 years ago in connection with the problem of radio wave propagation in the ionosphere [1 – 3]. Investigations have clarified the general patterns of wave propagation and interaction in the vicinity of the CS and have resulted in the calculation of transmission, reflection, and transformation coefficients for the waves incident upon the CS along the plasma density gradient. Numerical analysis of ray paths has revealed a number of their specific features, such as cusps (Spitzen) near the CS (see the paper [5] and also Refs [1, 4]). As noted in Ref. [6], a plasma opacity region that, generally speaking, exists in the vicinity of the CS disappears for waves that approach the CS with the wave vector parallel to the magnetic field vector. Such waves easily penetrate the CS. This effect was called the atmospheric 'radio window'. Electromagnetic waves pass through the radio window and penetrate into the dense plasma of the ionosphere. In the simplest plasma configurations, such as a plane layer with monotonically varying density, waves that pass through the radio window are slowed down as a result of a rather complex evolution and are eventually absorbed by the electron component of the plasma. It was proposed in the paper [7] to employ this effect for heating a dense plasma in magnetic

A V Timofeev Institute of Nuclear Fusion,
Russian Research Centre 'Kurchatov Institute',
pl. Kurchatova 1, 123182 Moscow, Russian Federation
Tel. (7-095) 196 91 83
E-mail: avtim@nfi.kiae.ru

Received 21 July 2003, revised 9 December 2003
Uspekhi Fizicheskikh Nauk **174** (6) 609 – 637 (2004)
Translated by Yu V Morozov; edited by A Radzig

traps making use of the so-called O-X-B scheme (O — ordinary, X — extraordinary, and B — Bernstein waves).

In more complicated situations, for example, in the presence of irregular inhomogeneities in the plasma, electromagnetic waves may be partly reflected and leave the plasma through the radio window. In this case, the plasma-reflected radio signal is trebled (see Refs [1–4, 6] and also Section 6.1).

These investigations received new impetus in the context of the thermonuclear problem, particularly in connection with the development of methods for the microwave heating of dense plasmas in magnetic traps (see, for instance, the above-mentioned work [7]). At the new stage, the theory on phenomena taking place in the vicinity of the CS was further developed. Transmission, reflection, and transformation coefficients were calculated for waves incident on the CS at some arbitrary angle to the density gradient [8–11]. The investigations covered the transmission of both plane waves and spatially restricted wave beams [12]. It was shown that the CS functions as a filter that transmits only part of the beam's Fourier spectrum from its expansion in respect to wave numbers. Wave polarization as well as its association with the specific features of ray paths near the CS, was analyzed in Ref. [12]. The passage of waves having a finite amplitude through the CS was considered in Ref. [13].

Some auxiliary results have been obtained in the above studies. It turned out that electromagnetic waves approaching the CS may be transformed into electron Langmuir oscillations with longitudinal (i.e., parallel to the principal direction of the magnetic field) polarization of the electric field. It is precisely this transformation that is responsible for the pointed shape of ray paths [12]. By virtue of the reversibility of the Maxwell equations, electron Langmuir oscillations must be back-transformed into electromagnetic waves. Because the latter can exit into a vacuum, the energy of electron Langmuir oscillations is converted into electromagnetic radiation energy [14, 15]. This mechanism manifests itself both in outer space and in laboratory experiments where rather intense electromagnetic radiation was not infrequently observed under conditions in which the theory predicts the development of Langmuir turbulence. The appearance of such radiation used to be ascribed to the nonlinear mechanisms of transformation of electron Langmuir oscillations into electromagnetic ones (see, for instance, Ref. [16]). In addition, a linear mechanism of transformation of short potential waves that can propagate under plasma resonance conditions in a magnetized plasma was considered in Refs [1–3].

Electromagnetic waves in the vicinity of the CS are subjected to strong refraction. Given a sufficiently large angle χ between the plasma density gradient and the direction of the magnetic field, such electromagnetic waves prove to be 'fastened' to the CS. This results in the formation of a wave channel adjacent to the CS in a plasma with monotonically changing density [17]. Waves localized in such a channel in a nonequilibrium plasma may lose stability and their amplitude becomes very large.

The objective of this review is to present a systematic analysis of the phenomena that occur during the propagation of electromagnetic waves near the CS. It was deemed convenient to represent the wave electric field as a sum of three components: one parallel to the main magnetic field vector, and two others normal to this vector and having opposite directions of rotation (i.e., right-handed polarized or electron component, and left-handed polarized or ion component). Such a representation is characteristic of the theory of cyclotron waves in a plasma (see, for instance, Ref. [18]) and has also been used in the analysis of electromagnetic waves near the CS (e.g., in Refs [7, 12, 13]). It helps to consider, in the framework of a simple mathematical model, the main physical process governing the propagation of electromagnetic waves in a magnetized plasma in the vicinity of a CS — that is, their interaction with natural plasma waves or electron Langmuir oscillations. This phenomenon also takes place in a nonmagnetized plasma, however, it is more efficacious in the presence of a magnetic field.

2. General wave pattern in a dense plasma in a magnetic field

For the analysis of waves in a magnetized plasma, the alternating electric field component normal to the main magnetic field vector can be represented as the superposition of circularly polarized fields $E_\pm = (E_x \pm \mathrm{i}E_y)/\sqrt{2}$, where $E_{x,y}$ are the components of the electric field in the right-handed Cartesian system of coordinates in which the Z-axis is parallel to the main magnetic field. If time dependence of alternating fields has the form $\propto \exp(-\mathrm{i}\omega t)$, components E_+ and E_- describe the electric fields that rotate to the left and right, respectively. In what follows, the sign combination $\pm$ used in subscripts to specify polarization of oscillations will be denoted by σ (e.g., $E_\pm = E_\sigma$), and that used in mathematical expressions by $\sigma = \pm 1$. The system of the Maxwell equations for a homogeneous cold plasma in terms of E_σ, $E_\parallel = E_z$ fields is reduced to an algebraic system of equations (see, for instance, Ref. [14])

$$\begin{pmatrix} N_\parallel^2 + N_+N_- - \varepsilon_+ & -N_+^2 & -N_\parallel N_+ \\ -N_-^2 & N_\parallel^2 + N_+N_- - \varepsilon_- & -N_\parallel N_- \\ -N_\parallel N_- & -N_\parallel N_+ & 2N_+N_- - \varepsilon_\parallel \end{pmatrix} \times \begin{pmatrix} E_+ \\ E_- \\ E_\parallel \end{pmatrix} = 0\,, \tag{2.1}$$

where $\mathbf{N} = \mathbf{k}c/\omega$ is the refractive index, then

$$N_\sigma = \frac{N_x + \mathrm{i}\sigma N_y}{\sqrt{2}}\,, \quad \varepsilon_\sigma = 1 - \frac{\omega_{\mathrm{pe}}^2}{\omega(\omega + \sigma\omega_{\mathrm{e}})}\,, \quad \varepsilon_\parallel = 1 - \frac{\omega_{\mathrm{pe}}^2}{\omega^2}\,,$$

and ω_{e} is the electron cyclotron frequency. The wave frequency is considered to be sufficiently high, and therefore the ionic contribution to the dielectric response of the plasma is disregarded. For the analysis of inhomogeneous plasma oscillations, the substitution $\mathbf{N} \to -\mathrm{i}\,\partial/\partial\mathbf{r}$ is needed in expression (2.1). Hereinafter, all quantities with the dimension of length are given in units of c/ω.

If the wavelength is small compared with the characteristic spatial scale of plasma inhomogeneity, the system of equations (2.1) defines local polarization of the electric field, with the refractive index becoming a function of coordinates. The solution to equations (2.1) has the form of the vector

$$\mathbf{E} = (E_+, E_-, E_\parallel) = \mathrm{const}\left(\frac{N_+}{\varepsilon_+ - N^2}\,, \frac{N_-}{\varepsilon_- - N^2}\,, \frac{N_\parallel}{\varepsilon_\parallel - N^2}\right). \tag{2.2}$$

The solution exists if the solvability condition for the system of equations (2.1), i.e., the dispersion relation [18]

$$D = 1 + \frac{N_\perp^2}{2}\left(\frac{1}{\varepsilon_+ - N^2} + \frac{1}{\varepsilon_- - N^2}\right) + \frac{N_\parallel^2}{\varepsilon_\parallel - N^2} = 0\,, \quad (2.3)$$

is satisfied. This relation can also be written in a familiar form, as the condition of polynomial in N^2 becoming zero (see, for instance, Ref. [19]):

$$D = N^4(\varepsilon_\perp \sin^2\theta + \varepsilon_\parallel \cos^2\theta) + N^2\left[(\varepsilon_\parallel - \varepsilon_\perp)\sin^2\theta - 2\varepsilon_\perp\varepsilon_\parallel\right] + \varepsilon_+\varepsilon_-\varepsilon_\parallel = 0\,, \quad (2.4)$$

where $\varepsilon_\perp = (\varepsilon_+ + \varepsilon_-)/2$, and θ is the angle between the wave and magnetic field vectors.

Equations (2.3) and (2.4) are equivalent. It may be more convenient to use one or the other for the purpose of a concrete task.

In the absence of a magnetic field, all constituents of the permittivity tensor, regardless of their index, are equal to $\varepsilon = 1 - (\omega_{pe}/\omega)^2$, and the dispersion relation (2.4) acquires the form

$$D = \varepsilon(N^2 - \varepsilon)^2 = 0\,.$$

Hence it follows that the condition $\varepsilon = 0$ performs two functions. First, it defines the maximum density above which the plasma cannot be transparent for electromagnetic waves (the cut-off condition). Second, it allows the frequency of natural plasma oscillations (i.e., electron Langmuir oscillations) to be determined. For these oscillations $\mathbf{E} \propto \mathbf{N}$, in accordance with expression (2.2), thus reflecting the potential character of the electric field [1]. Notice that it is inconvenient to use formula (2.2) for the determination of polarization of electromagnetic waves in a nonmagnetized plasma and in the passage to the vacuum limit in the magnetized plasma, because Eqn (2.2) gives rise to divergent expressions.

Plasma embedded in a magnetic field is anisotropic and gyrotropic, its dielectric properties being characterized by three quantities: $\varepsilon_\pm$, and $\varepsilon_\parallel$. The refractive index of waves traveling in such plasma vanishes together with one of these quantities — the cut-off condition [see formula (2.4)]. It is noteworthy that the plasma response (ε_-) to a right-handed polarized field for $\omega < \omega_e$ is positive at any plasma density. This suggests the possibility of propagation of right-handed polarized waves (helicons) in a plasma of arbitrarily high density (see below).

It follows from relationship (2.2) that, in a plasma placed in a magnetic field, natural plasma waves with a potential electric field can exist only in the limit $N \to \infty$. Their frequency, in conformity with expression (2.4), is determined by the condition

$$\varepsilon_\perp \sin^2\theta + \varepsilon_\parallel \cos^2\theta = 0\,. \quad (2.5)$$

Unlike the case of a nonmagnetized plasma, condition (2.5) coincides with one of the cut-off conditions, $\varepsilon_\parallel = 0$, only for waves traveling parallel to the magnetic field. It will be shown below that an inhomogeneous plasma with such waves undergoing transformation into electron Langmuir oscillations gives rise to interesting physical effects, the analysis of which constitutes one of the main subjects of the present review.

The general notion of the properties of dense plasma waves ($\omega_{pe} \geqslant \omega$) in a magnetic field can be inferred from the analysis of the $N^2(\omega_{pe}^2)$ dependence at different values of the angle θ between the oscillation wave vector and the magnetic field vector.

The matrix in the left-hand side of Eqn (2.1) becomes diagonal at $\theta = 0$ ($N_\perp = 0$), and the system of equations (2.1) breaks down into three independent equations corresponding to three different wave branches, namely

$$(N^2 - \varepsilon_\sigma)E_\sigma = 0\,, \quad (2.6)$$

$$\varepsilon_\parallel E_\parallel = 0\,. \quad (2.7)$$

Waves are frequently classified based on their polarization patterns during the propagation across ($\theta = \pi/2$) a magnetic field (see, for instance, Ref. [19]). Those having the linearly polarized electric vector are referred to as ordinary, and those with the transversely polarized electric vector as extraordinary. In a low-density plasma with $q_e = (\omega_{pe}/\omega)^2 < 1$, waves of the former type in the limit of $\theta = 0$ are converted into waves whose electric vector rotates to the left ($N^2 = \varepsilon_+$). Under the same conditions ($\theta = 0$), waves of the latter type have an electric vector that rotates to the right ($N^2 = \varepsilon_-$) [see Eqn (2.6)]. When plasma density exceeds a critical value ($q_e > 1$), the direction of rotation of the electric vector of extraordinary waves at $\theta = 0$ undergoes left-for-right reversal. Waves with the vector rotating to the right cannot be classified as ordinary or extraordinary because it is impossible to extend them to the angle $\theta = \pi/2$, because for a given wave branch there is a limiting angle θ_s between vectors $\mathbf{N}$ and $\mathbf{B}_0$ (see below).

For this reason, the traditional classification of waves as ordinary and extraordinary ones in the vicinity of the CS, where $q_e \approx 1$, would be inconvenient for their analysis. In what follows, the main focus of attention will be waves propagating at a small angle to the magnetic field vector, for which $N^2 \approx \varepsilon_+$ or $N^2 \approx \varepsilon_-$ and which easily penetrate the CS (see below). The former will be referred to as left-handed polarized, and the latter as right-handed polarized. These definitions are, to a large degree, conventional because the electric field of either wave type in the vicinity of a CS at $\theta \neq 0$ has not only a circular component but also a longitudinal one of comparable value that, under certain conditions, can even predominate.

It is worthwhile to note that, in the analysis of circularly polarized waves using Eqns (2.2) and (2.3), a case of $\theta = 0$ should be considered as the limiting one at $\theta \to 0$. In this case, the use of relation (2.3) yields $N^2 = \varepsilon_\sigma + O(\theta^2)$ and, in accordance with Eqn (2.2), one of the circular constituents of the electric vector actually becomes predominant, namely

$$E_\sigma \propto \theta^{-1} \underset{\theta \to 0}{\to} \infty\,.$$

Equation (2.7) shows that, similar to the situation with the absence of a magnetic field, the plasma exhibits 'natural', resonance frequency, i.e., the frequency of potential electron Langmuir oscillations whose electric field is parallel to the main magnetic field. Because in the cold plasma approximation their refractive index may acquire any value, the dispersion dependence of electron Langmuir oscillations in the (q_e, N^2)-plane has the form of a vertical straight line $q_e = 1$ (Figs 1a and 2a).

As electromagnetic waves traverse the CS, their resonance interaction with the plasma should be expected to occur

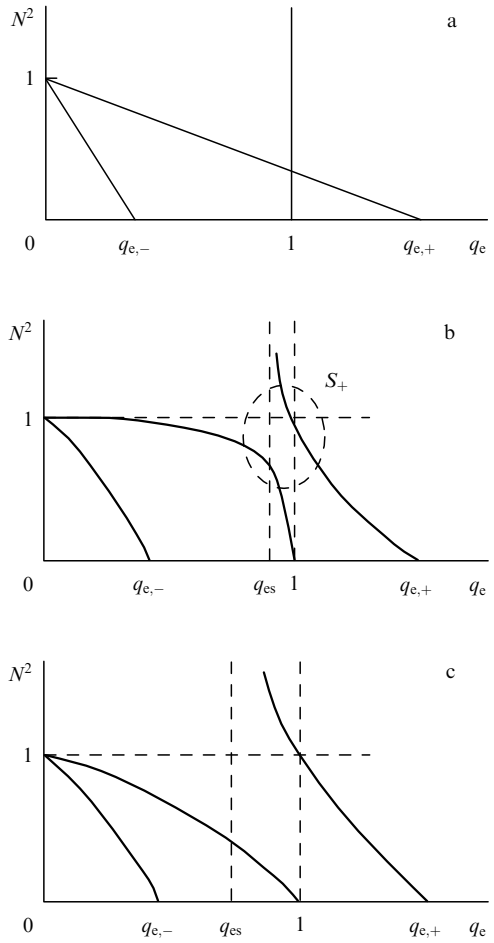

Figure 1. Plasma density dependence of the refractive index at $\Omega_e = \omega_e/\omega < 1$: (a) $\theta = 0$, (b) $\theta \ll 1$, (c) $\theta \leqslant \pi/2$; S_σ are the areas of interaction of different wave modes $q_{e,\sigma} = 1 + \sigma\Omega_e$.

similar, for example, to cyclotron resonance in a nonuniform magnetic field. However, the electric field of electron Langmuir oscillations is orthogonal to that of electromagnetic waves propagating parallel to the main magnetic field (see above). Due to this, the electromagnetic waves at $\theta = 0$ freely penetrate the CS and their dispersion dependences intersect the vertical line $q_e = 1$ in the (q_e, N^2)-plane (Figs 1a and 2a).

The situation described in the preceding paragraph is somewhat reminiscent of cyclotron resonance $(\omega = \omega_j, j = e, i)$ in a cold plasma where electromagnetic waves propagate at some angle to the magnetic field $(\theta \neq 0)$. Such waves do not 'notice' the resonance surface, $\omega = \omega_j(\mathbf{r})$, because the circular component of the electric field, rotating in the same direction as j-type particles, turns to zero at this surface (see, for instance, Ref. [18]).

Another analog is the problem of incidence of an electromagnetic S-wave upon a plane layer of a nonmagnetized plasma. The electric field of such a wave is normal to the plasma density gradient; hence, for reasons of symmetry, it cannot excite electron Langmuir oscillations (see, for example, Refs [1 – 3] and also Section 4).

Now, let us suppose that the wave vector of electromagnetic waves deflects from the direction of the magnetic field. In this case, the alternating electric field possesses a longitudinal component, which leads to the interaction with

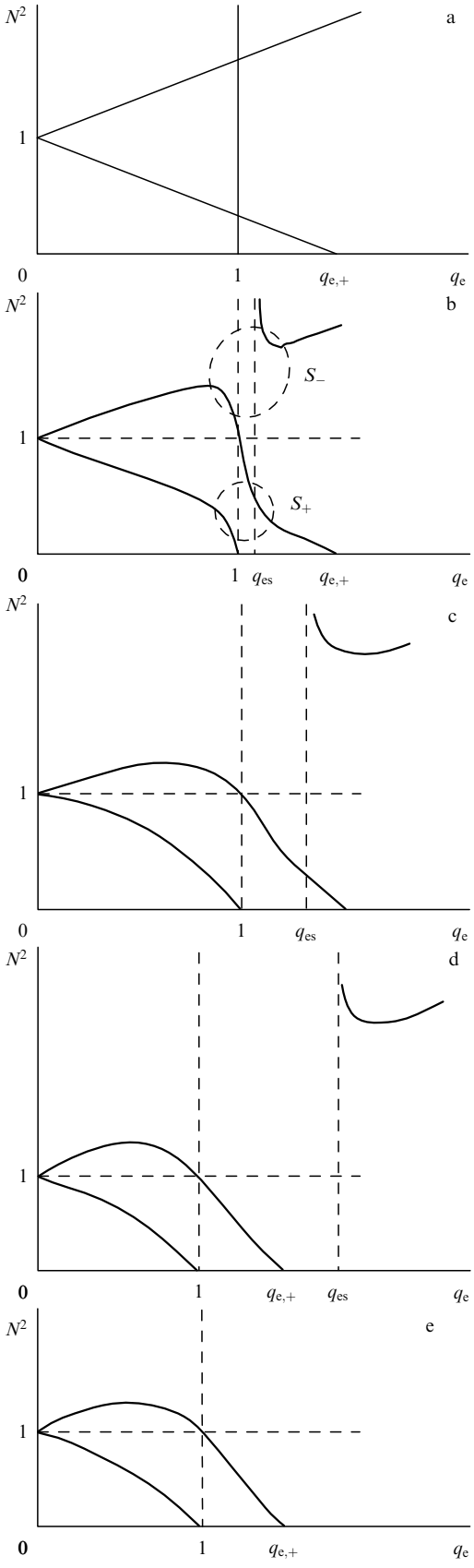

Figure 2. Plasma density dependence of the refractive index at $\Omega_e > 1$: (a) $\theta = 0$, (b) $\theta \ll 1$, (c) $\cos\theta > \Omega_e^{-1/2}$, (d) $\Omega_e^{-1/2} > \cos\theta > \Omega_e^{-1}$, (e) $\Omega_e^{-1} > \cos\theta$. Notations are the same as in Fig. 1.

electron Langmuir oscillations. For its description on the assumption of $N_\perp \ll N_\parallel$, matrix (2.1) must retain elements proportional to the first power of the refractive index components orthogonal to $\mathbf{B}_0$. In the region of $N^2 \approx \varepsilon_\sigma$, $q_e \approx 1$, the system of equations (2.1) yields

$$\begin{pmatrix} -N_\parallel^2 + \varepsilon_\sigma & N_\sigma N_\parallel \\ N_{-\sigma} N_\parallel & \varepsilon_\parallel \end{pmatrix} \begin{pmatrix} E_\sigma \\ E_\parallel \end{pmatrix} = 0 . \tag{2.8}$$

The solvability condition for the system of equations (2.8) has the form

$$\varepsilon_\parallel (N_\parallel^2 - \varepsilon_\sigma) + \frac{1}{2} N_\perp^2 \varepsilon_\sigma = 0 . \tag{2.9}$$

Obviously, both relationships (2.3) and (2.4) can be reduced to Eqn (2.9).

It will be shown below that the system of equations (2.8) and dispersion relation (2.9) permit us to obtain basic information about wave properties in the vicinity of a CS (polarization, shape of ray paths, transmission and reflection coefficients, etc.).

In the analysis of homogeneous plasma waves, Eqn (2.9) can be conveniently represented in the form

$$N^2 \approx \varepsilon_\sigma - \frac{\varepsilon_\sigma^2}{2\varepsilon_\parallel} \theta^2 . \tag{2.10}$$

In agreement with what has been said above, the CS, on which $\varepsilon_\parallel = 0$, actually appears in expression (2.10) as a resonance surface. As the surface is approached, the difference $N^2 - \varepsilon_\sigma$ strikingly increases. As a result, the dispersion dependences take a characteristic 'resonant' form with a discontinuity at a critical value of $q_e = 1$ (Figs 1b and 2b). Selected portions of the broken vertical line $q_e = 1$ describing waves similar to electron Langmuir oscillations in the (q_e, N^2)-plane combine with the dispersion dependences for circularly polarized waves. Such a combination reflects the possibility of a radical change in wave nature, namely, transformation of circularly polarized electromagnetic waves incident on the CS into waves resembling electron Langmuir (quasi-potential) oscillations. The main constituent of the electric field in such waves is longitudinal. Certainly, the process may proceed in the opposite direction.

The property of exact potentiality at $\theta \neq 0$ passes over to the waves with $N \to \infty$, the frequency of which, according to relation (2.2), must satisfy condition (2.5). Such waves are described as experiencing the plasma (upper hybrid) resonance (UHR).

At fixed ω and θ, Eqn (2.5) gives the resonant value of q_e:

$$q_{es} = \frac{1 - \Omega_e^2}{1 - \Omega_e^2 \cos^2 \theta} , \tag{2.11}$$

where $\Omega_e = \omega_e/\omega$.

Under condition $\theta \ll 1$, Eqn (2.11) yields

$$q_{es} \approx 1 + \frac{\Omega_e^2}{\Omega_e^2 - 1} \frac{\theta^2}{2} . \tag{2.12}$$

The surface at which condition (2.5) is satisfied in an inhomogeneous plasma is referred to as the plasma resonance surface. Upon approaching this surface, the refractive index grows indefinitely, and the corresponding dispersion curve has a vertical asymptote in the (q_e, N^2)-plane (see Figs 1 and 2).

In another limiting case of transverse propagation ($\theta \to \pi/2$, $N_\parallel \to 0$), the complete dispersion relation for $\omega > \omega_{pe}$ ($q_e < 1$) has two solutions: $N^2 = \varepsilon_\parallel + O(\cos^2 \theta)$ and $N = \varepsilon_+ \varepsilon_- / \varepsilon_\perp$ (Figs 1c and 2d). The first one characterizes ordinary waves whose electric field is parallel to the main magnetic field, while the second one characterizes extraordinary waves with $\mathbf{E} \perp \mathbf{B}_0$. In a dense plasma ($\omega < \omega_{pe}$), only extraordinary waves can propagate normally to the magnetic field vector. The dispersion dependences for intermediate angles $0 < \theta < \pi/2$ are also shown in Figs 1 and 2. They permit us to naturally link the limiting cases of longitudinal ($\theta = 0$) and transverse ($\theta = \pi/2$) wave propagation.

It can be seen from Fig. 2 that the transparent region for waves with $\omega < \omega_e$ is not restricted on the high-density side. Such waves are called helicons or whistlers. Their dispersion dependence for $q_e \gg 1$, obtainable from Eqns (2.1) and (2.2), has a rather simple form (see, for instance, Ref. [19])

$$N^2 \approx \frac{\omega_{pe}^2}{\omega(\omega_e \cos \theta - \omega)} . \tag{2.13}$$

It is worthwhile to note that the angle θ for helical waves cannot be too large. Its limiting value θ_s varies from zero near the critical surface to $\theta_s = \arccos(\omega/\omega_e)$ for $q_e \to \infty$ [see formulas (2.5) and (2.11)]. At $\theta = \theta_s$, the helicons undergo plasma resonance (see above).

Using helical waves, it is possible to obtain gas discharges in which plasma density is substantially higher than the critical one. Extensive studies of such discharges, referred to as helicon charges, are underway (see, e.g., Ref. [20]).

Extraordinary waves (see above) differing from helicons can also propagate beyond the critical surface. However, they do not penetrate too deep into the dense plasma: $q_e < q_{e,+} = 1 + \Omega_e$. Their refractive index at the CS equals unity regardless of the value of the angle θ, as is obvious from the dispersion relation in the form of Eqn (2.4). This property likens these waves to electromagnetic waves in a vacuum. At the same time, it is easy to demonstrate that their polarization differs from vacuum polarization, and group velocity is not coincident with phase velocity. Under certain conditions, these waves are involved in a complex sequence of processes ending in the absorption of electromagnetic waves incident on the dense plasma (O-X-B heating, see Section 9.2).

The entire set of dependences presented in Figs 1 and 2 can be replaced by a single Clemmow–Mullaly–Allis (CMA) diagram (see, for instance, Refs [19, 21]).

3. Plane-layered plasma waves with the wave vector closely aligned with the magnetic field vector, near the critical surface

3.1 Transparent regions

The most complicated and interesting wave phenomena take place in a thin layer of inhomogeneous plasma, including the CS. The curvature of the CS within this layer is often insignificant, and therefore a reasonable plane layer model is that in which plasma density is linearly dependent on the coordinates. In the (ξ, ζ)-coordinate system presented in Fig. 3, the 0ξ-axis is oriented along the density gradient and $n_0(\mathbf{r}) = n_{00}(1 + \xi/L)$, where L is the characteristic scale of plasma density variation, and n_{00} is the plasma density at $\xi = 0$. It is assumed that the plane $\xi = 0$ coincides with the

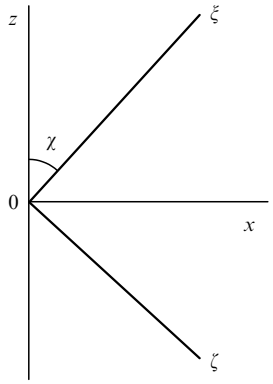

Figure 3. Coordinate systems used in this review.

CS. As waves propagate over a plane-layered plasma, components N_ζ, N_y of the refractive index orthogonal to the density gradient are conserved.

The results presented in Section 2 hold true for waves having $N_\zeta = N_y = 0$ ($\mathbf{N} \parallel \nabla n_0$). However, the waves with the nonparallel vectors $\mathbf{N}$, ∇n_0 are also rather interesting. Most essential that such waves can easily penetrate the CS at nonzero values of the angle χ between ∇n_0 and $\mathbf{B}_0$ [1, 6]. It follows from the discussion in Section 2 that such a situation is feasible if the wave vector at the CS itself is parallel to the magnetic field vector. In this case, $N^2 = \varepsilon_\sigma$, $N_\xi = \sqrt{\varepsilon_{\sigma,\mathrm{c}}}\cos\chi$, $N_\zeta = \sqrt{\varepsilon_{\sigma,\mathrm{c}}}\sin\chi$, and $N_y = 0$, where $\varepsilon_{\sigma,\mathrm{c}} = \Omega_\mathrm{e}/(\Omega_\mathrm{e} + \sigma)$ is the value of the dielectric response ε_σ on the CS, i.e., at $q_\mathrm{e} = 1$. If waves with the above values of N_y, N_ζ (called optimal here) are excited in front of the CS, the equality $N_\xi = \sqrt{\varepsilon_{\sigma,\mathrm{c}}}\cos\chi$ (with $\mathbf{N} \parallel \mathbf{B}_0$) must be fulfilled at this surface by virtue of unique solution to the dispersion equation.

Let us analyze now waves that have the wave vector in the vicinity of the CS slightly deflecting from the direction of the magnetic field; as pointed out above, these waves easily penetrate the CS. Such waves are described by the approximate system of equations (2.8), the solvability condition of which takes the form (2.9). This equation governing the interaction of electron Langmuir oscillations with circularly polarized waves permits us to reveal major wave peculiarities near the CS.

Assuming

$$N_x = N_\xi \sin\chi - N_\zeta \cos\chi\,, \qquad N_z = N_\xi \cos\chi + N_\zeta \sin\chi\,,$$
$$\varepsilon_\parallel \approx \delta q_\mathrm{e}\,, \qquad \varepsilon_\sigma \approx \varepsilon_{\sigma,\mathrm{c}} - \sigma\,\frac{\delta q_\mathrm{e}}{\Omega_\mathrm{e} + \sigma}\,,$$
$$N_\parallel^2 \approx \varepsilon_{\sigma,\mathrm{c}} + 2\sqrt{\varepsilon_{\sigma,\mathrm{c}}}\,(\delta N_\xi \cos\chi + \delta N_\zeta \sin\chi)\,,$$
$$N_\perp^2 \approx (\delta N_\xi \sin\chi - \delta N_\zeta \cos\chi)^2 + N_y^2\,,$$
$$\delta N_\xi = N_\xi - \sqrt{\varepsilon_{\sigma,\mathrm{c}}}\cos\chi\,, \qquad \delta N_\zeta = N_\zeta - N_{\zeta,\sigma}^{\mathrm{opt}}\,,$$
$$N_{\zeta,\sigma}^{\mathrm{opt}} = \sqrt{\varepsilon_{\sigma,\mathrm{c}}}\sin\chi$$

in Eqn (2.9) leads to the quadratic equation for δN_ξ:

$$(\delta N_\xi \sin\chi)^2 - 2\delta N_\xi \cos\chi\left(\frac{2\delta q_\mathrm{e}}{\sqrt{\varepsilon_{\sigma,\mathrm{c}}}} + \delta N_\zeta \sin\chi\right)$$
$$- \sigma\,\frac{2\delta q_\mathrm{e}^2}{\Omega_\mathrm{e}} - 4\delta q_\mathrm{e}\,\delta N_\zeta\,\frac{\sin\chi}{\sqrt{\varepsilon_{\sigma,\mathrm{c}}}} + (\delta N_\zeta \cos\chi)^2 + N_y^2 = 0\,. \quad (3.1)$$

The complete dispersion relation describing waves in a plane-layered plasma has the fourth degree in N_ξ (Booker's quadric [22]). It was replaced by a simplified dispersion relation of the second degree, for instance, in Refs [23, 24].

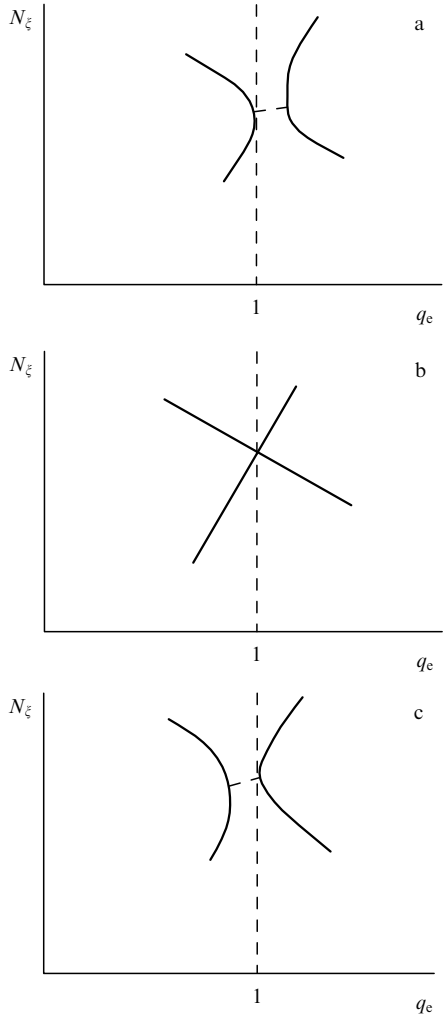

Figure 4. Dispersion dependence for left-handed polarized waves in a plane plasma layer near the CS at $N^2 \approx \varepsilon_+$: (a) $\delta N_\zeta < 0$, (b) $\delta N_\zeta = 0$, and (c) $\delta N_\zeta > 0$.

The nontransparent region for the waves under consideration is defined by the condition that the discriminant G of equation (3.1) is negative:

$$G = 2\delta q_\mathrm{e}^2\,\frac{1}{\Omega_\mathrm{e}}\,g_\sigma(\Omega_\mathrm{e}, \chi) + 4\delta q_\mathrm{e}\sin\chi\,\frac{\delta N_\zeta}{\sqrt{\varepsilon_{\sigma,\mathrm{c}}}} - N_y^2\sin^2\chi < 0\,, \quad (3.2)$$

where $g_\sigma(\Omega_\mathrm{e}, \chi) = 2(\Omega_\mathrm{e} + \sigma)\cos^2\chi + \sigma\sin^2\chi$.

The nontransparent region for $N_y \neq 0$ includes the CS; it becomes smaller as $|N_y|$ decreases. For waves with $N_y = 0$, the CS makes one of the boundaries of the nontransparent region. Its other boundary lies in the higher-density region ($\delta q_\mathrm{e} > 0$) for $\delta N_\zeta < 0$, and in the lower-density region ($\delta q_\mathrm{e} < 0$) for $\delta N_\zeta > 0$. Within the nontransparent region, the quantity δq_e varies from zero to $\delta q_{\mathrm{e},1}$, with

$$\delta q_{\mathrm{e},1} = -\frac{2\delta N_\zeta \Omega_\mathrm{e}^2}{\sqrt{\varepsilon_{\sigma,\mathrm{c}}}}\,\frac{\sin\chi}{g_\sigma(\Omega_\mathrm{e},\,\chi)}\,. \quad (3.3)$$

Characteristic dispersion dependences in the vicinity of the CS are depicted in Figs 4 and 5. The nontransparent

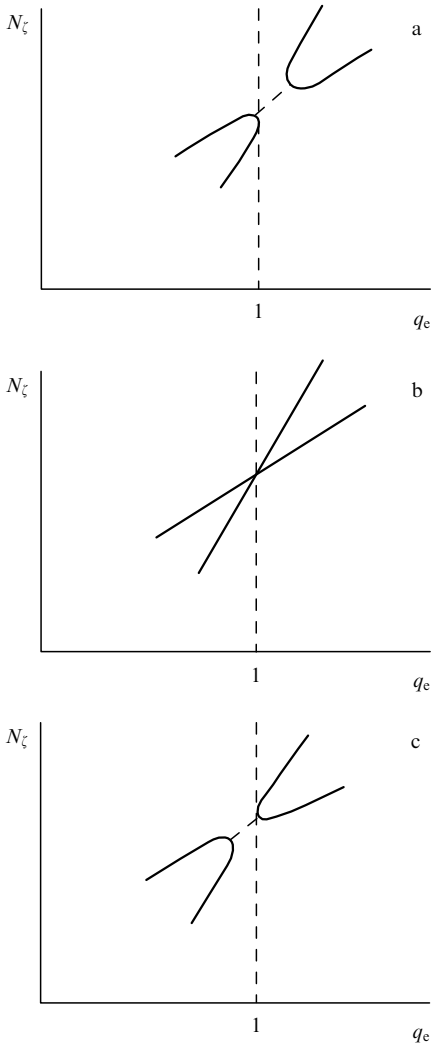

Figure 5. Dispersion dependence for right-handed polarized waves in a plane plasma layer near the CS as $N^2 \approx \varepsilon_-$, $\chi < \chi_{\max}$: (a) $\delta N_\zeta < 0$, (b) $\delta N_\zeta = 0$, and (c) $\delta N_\zeta > 0$.

region broadens as angle χ increases. For right-handed polarized waves (helicons), the maximum value of the angle χ is given by

$$\chi_{\max} = \arccos\left(2\Omega_e - 1\right)^{-1/2}, \tag{3.4}$$

at which the quantity $g_\sigma(\Omega_e, \chi)$ vanishes. In this case, the nontransparent region occupies the entire half-space $\delta q_e\, \delta N_\zeta < 0$. Certainly, this statement holds only for the range of applicability of the approximate dispersion relation (3.1), which is restricted by the condition $|\delta q_e| \ll 1$.

When the angle $\chi > \chi_{\max}$, the situation reverses for right-handed polarized waves or helicons ($\sigma = -$). Specifically, regions lying far from the CS become nontransparent, whereas a channel appears near the CS through which helical waves may propagate [19]. One of the boundaries for this channel at $N_y = 0$ is formed by the CS. The width of the channel tends to zero, and it contracts to the CS at $\delta N_\zeta = 0$ (Fig. 6). It is important that the wave channel exists in a situation of monotonically varying density.

For right-handed polarized waves in a plane-layered plasma, there is one more critical value of the angle:

$$\chi_{\rm cr} = \arccos\left(\Omega_e^{-1/2}\right) < \chi_{\max}.$$

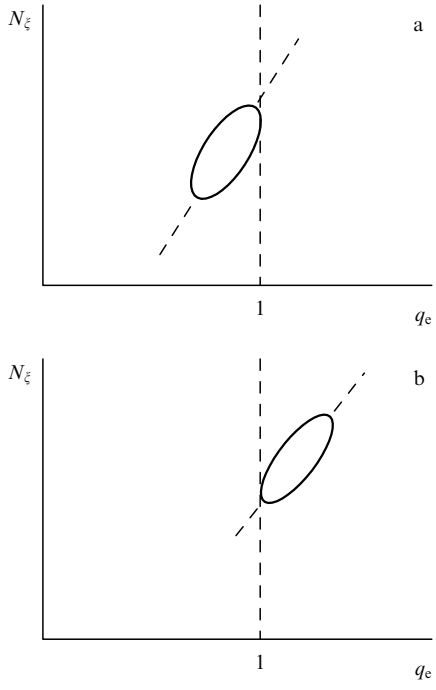

Figure 6. Dispersion dependence for right-handed polarized waves in a plane plasma layer near the CS as $N^2 \approx \varepsilon_-$, $\chi > \chi_{\max}$: (a) $\delta N_\zeta < 0$, and (b) $\delta N_\zeta > 0$.

If the angle $\chi > \chi_{\rm cr}$, then $N_{\zeta,-}^{\rm opt} = \varepsilon_{-,c}^{1/2} \sin\chi > 1$. This makes impossible the launching of waves with $N_\zeta = N_{\zeta,-}^{\rm opt}$ from the vacuum, the waves that could be able to penetrate the CS without obstacle. There is no limitation on the angle χ for left-handed polarized waves.

3.2 Wave polarization

Waves with $N^2 \approx \varepsilon_{\sigma,c}$, $N_y \to 0$ easily penetrating through the CS possess rather peculiar polarization in the vicinity of this surface. Their electric field is dominated by the constituents E_σ, $E_\parallel$. Using relations (2.2) and (2.8) at $N_y = 0$, it is found that

$$\frac{E_\parallel}{E_\sigma} = \frac{N_x \varepsilon_{\sigma,c}^{1/2}}{2\delta q_e}. \tag{3.5}$$

It should be recalled that the x coordinate is normal to the magnetic field.

In order to find N_x, the dispersion relation (3.1) needs to be rewritten in the form

$$N_x^2 + N_y^2 - 4\,\frac{\delta q_e}{\varepsilon_{\sigma,c}^{1/2}}\cot\chi N_x - 2\delta q_e\left(\frac{2\delta N_\zeta}{\varepsilon_{\sigma,c}^{1/2}\sin\chi} + \frac{\sigma}{\Omega_e}\,\delta q_e\right) = 0. \tag{3.6}$$

For waves with $N_y = \delta N_\zeta = 0$ easily penetrating the CS, from this it follows that

$$\frac{N_x}{\delta q_e} = \frac{2\cot\chi}{\varepsilon_{\sigma,c}^{1/2}} \pm \left(\frac{4\cot^2\chi}{\varepsilon_{\sigma,c}} + \frac{2\sigma}{\Omega_e}\right)^{1/2}, \tag{3.7}$$

and hence

$$\frac{E_\parallel}{E_\sigma} = \cot\chi \pm \left[\cot^2\chi + \frac{\sigma}{2(\Omega_e + \sigma)}\right]^{1/2}. \tag{3.8}$$

Here, the '±' signs characterize the direction of wave propagation.

In the particular case of $\chi = \pi/2$, when only left-handed polarized waves ($\sigma = +$) can penetrate the CS (see Section 3.1), Eqn (3.8) yields $E_\parallel/E_+ = [2(\Omega_e + 1)]^{-1/2}$ [12]. This means that waves at the CS itself are actually a superposition of circularly polarized waves and electron Langmuir oscillations. It has been shown in Refs [1, 6] that the refractive index of such waves at the CS is parallel to the magnetic field vector and equal to $N = \varepsilon_\sigma^{1/2}$. The electric field of these waves should be a circularly polarized one ($E = E_\sigma$) everywhere outside the CS.

It follows from relationship (3.6) that for $\delta N_\zeta \neq 0$ near the CS the following passages to the limit occur:

$$N_x \to 2\left(\frac{\delta q_e\, \delta N_\zeta}{\varepsilon_{\sigma,c}^{1/2} \sin\chi}\right)^{1/2}, \qquad N_\parallel \to \sqrt{\varepsilon_{\sigma,c}} + \frac{\delta N_\zeta}{\sin\chi}\,.$$

At the CS itself, the electric field becomes purely longitudinal, in conformity with Eqn (3.5). Such waves should be regarded as electron Langmuir oscillations. Indeed, only electron Langmuir oscillations have the frequency ω_{pe}, regardless of the refractive index value, and their electric field is longitudinal.

Thus, it may be concluded that electromagnetic waves propagating in an inhomogeneous plasma placed in a magnetic field undergo transformation into electron Langmuir oscillations at the CS [12]. Certainly the reverse statement is true — that is, electron Langmuir oscillations are transformed into electromagnetic waves as the distance from the CS increases. It should be recalled that the CS forms a boundary of the nontransparent region for electromagnetic waves having $N_y = 0$. Wave propagation near this boundary will be a subject of detailed analysis in Section 4.

It follows from relationship (3.6) that at $N_y = 0$ the quantity $N_\perp = |N_x|$ vanishes completely both at the CS ($\delta q_e = 0$) and at a surface where

$$\delta q_e(\xi) = \delta q_{e,2} = -\frac{2\Omega_e\, \delta N_\zeta}{\sigma \varepsilon_{\sigma,c}^{1/2} \sin\chi}\,.$$

In accordance with condition (3.4) [see also the original dispersion equation (2.9)], $N_x \propto \delta q_e - \delta q_{e,2}$, and $N^2 - \varepsilon_\sigma \propto N_x^2$ in the vicinity of this surface. Therefore, waves approaching it turn to be circular polarized [see formula (2.2)]. Taking into consideration Eqn (3.3), it is easy to demonstrate that this surface is localized in the transparent region and coincides with its boundary at $\chi = \pi/2$. It was shown in Section 3.1 that the other boundary of the nontransparent region is formed by the CS. This accounts for drastic changes in the characteristics of waves with $N_y = 0$ at $\chi = \pi/2$ during their passage through the nontransparent region. These waves have the form of potential electron Langmuir oscillations on one boundary (CS) of the nontransparent region, and the form of circularly polarized electromagnetic waves on its other boundary and vice versa.

For helical waves at $\chi > \chi_{max}$, where χ_{max} is determined by condition (3.4), the transparent region has the form of a wave channel near the CS (see Section 3.1). In the case of $\chi = \pi/2$, helicons oscillate between the channel walls and alternately take the form of electron Langmuir oscillations and circularly polarized electromagnetic waves.

3.3 Waves at a small angle between the plasma density gradient and magnetic field vector. General pattern of wave propagation in a plane-layered plasma near the critical surface

Wave interactions in the vicinity of a CS become more complicated as the angle χ decreases. In the first place, the size of the nontransparent region near the CS is reduced as $\chi \to 0$, in conformity with Eqn (3.3). Simultaneously, the 'optimal' values $N_{\zeta,\sigma}^{opt}$ become small for both left-handed ($\sigma = +$) and right-handed ($\sigma = -$) polarized waves. This enables waves of the two types with the same value of $N_\zeta \ll 1$ to effectively penetrate the CS.

Secondly, the plasma resonance surface comes close to the CS and its position can be deduced from the following considerations. Only one component N_ξ of the refractive index varies during wave propagation over a plane-layered plasma. It grows indefinitely with the approach to the plasma resonance surface; hence, the angle θ between the vectors $\mathbf{N}$ and $\mathbf{B}_0$ tends to χ. Therefore, the resonant value of plasma density is determined by relations (2.11) and (2.12) in which $\theta = \chi$. It is found using formula (2.12) that the critical and resonance surfaces are close to each other ($|q_{es} - 1| \ll 1$) if the condition $L\chi^2 \ll 1$ is satisfied. Due to the proximity to the plasma resonance surface, plasma waves undergo very strong perturbation leading to a change in their behavior. Specifically, it affects the form of the dispersion dependences obtained from Eqn (3.1). Upon removal from the CS ($q_e = 1$) in the $q_e N_\xi$-plane, they asymptotically tend to straighten. One of them is almost vertical for $\chi \ll 1$:

$$\delta N_\xi \approx \frac{4}{\varepsilon_{\sigma,c}^{1/2} \chi^2}\, \delta q_e\,.$$

Using the system of equations (2.8) and taking into consideration formula (3.8), it is found that $E_\parallel/E_\sigma \approx 2/\chi$ for the respective waves; hence, they resemble electron Langmuir oscillations. Indeed, it was assumed above that $N_\parallel \gg N_\perp$ and $\omega_{pe} \approx \omega$. Let us recall that electron Langmuir oscillations on the $q_e N_\xi$-plane are depicted by a vertical straight line $q_e = 1$. We shall call the waves being discussed quasi-potential waves.

The slope of the second asymptote deduced from Eqn (3.1) is significantly smaller, so that

$$\delta N_\xi \approx -\sigma\, \frac{2\varepsilon_{\sigma,c}^{1/2}}{\Omega_e}\, \delta q_e\,.$$

Polarization of the corresponding waves is close to circular, since for them $N^2 \approx N_\parallel^2 \approx \varepsilon_\sigma(\xi)$.

Waves incident upon the CS and reflected from it are associated with different asymptotes on the $q_e N_\xi$-plane. It follows from the aforesaid that the reflection for $\chi \ll 1$ results in a dramatic change of the wave character — that is, circularly polarized waves undergo transformation into quasi-potential ones and vice versa. It will be shown below that as $\omega_e > \omega$ the circularly polarized waves having electric vectors with different directions of rotation near the CS are interconvertible via an intermediate stage of quasi-potential waves.

In order to analyze processes taking place in the vicinity of the CS for $\chi \ll 1$, it is necessary to go beyond the assumption used to derive Eqn (3.1) — that is, to take into consideration all the three constituents $(E_\pm, E_\parallel)$ of the alternating electric field. To this effect, the first equation of the simplified system (2.8) can be used with both σ values, as before. However, the

last equation of this system should be substituted by the last equation of the original complete system (2.1). The solvability condition for the modified system of equations is obtained by generalization of the dispersion relation (2.9):

$$(N_\parallel^2 - \varepsilon_+)(N_\parallel^2 - \varepsilon_-)\varepsilon_\parallel + N_\perp^2(N_\parallel^2 - 1)\varepsilon_\perp = 0\,. \tag{3.9}$$

As the angle χ decreases, the size of the regions $S_\sigma^\pm$ near the CS, in which the processes of interest proceed, is also reduced. It follows, in particular, from Eqns (3.1)–(3.3). As a result, terms $\propto (\delta q_e)^2$ taking into account the dependence of ε_σ on the ξ coordinate in relation (3.9) can be omitted for $\chi \ll 1$. Assuming $\varepsilon_\sigma = \varepsilon_{\sigma,c}, \varepsilon_{\perp,c} = \Omega_e^2/(\Omega_e^2 - 1), \varepsilon_\parallel = 1 - q_e = -\delta q_e$, $\sin\chi \approx \chi$, and $\cos\chi \approx 1$ in the dispersion relation (3.9), it can be given in the form

$$\delta q_e \approx \varepsilon_{\perp,c}\,\frac{\left[(\chi N_\xi - N_\zeta)^2 + N_y^2\right](N_\xi^2 - 1)}{(N_\xi^2 - \varepsilon_{+,c})(N_\xi^2 - \varepsilon_{-,c})}\,. \tag{3.10}$$

Expression (3.10) defines the dependence $\delta q_e(N_\xi)$, the inverse of the dispersion dependence $N_\xi(q_e)$. If the components $N_\zeta \approx \chi\sqrt{\varepsilon_{\sigma,c}}$, $N_y = 0$, then $N_\xi \approx \sqrt{\varepsilon_{\sigma,c}}$, and expression (3.10) takes the form

$$\delta q_e \approx \frac{1}{4}\,\chi^2\sqrt{\varepsilon_{\sigma,c}}\,\frac{(N_\xi - N_\zeta/\chi)^2}{N_\xi - \sqrt{\varepsilon_{\sigma,c}}}\,. \tag{3.11}$$

It is easy to show that relationship (3.11) coincides with Eqn (3.1) if we set $\chi \ll 1$ in the latter and the term $\propto (\delta q_e)^2$ is omitted.

The dependences (3.10) and (3.11) may be helpful to fully describe the evolution of the dispersion curves on the (q_e, N_ξ)-plane at varying N_ζ. In what follows, it is analyzed in more detail for a simpler case of waves with $\omega > \omega_e$, when only left-handed polarized waves can penetrate the CS.

When $\mathbf{N} \parallel \nabla n_0$ $(N_y = N_\zeta = 0)$, the waves propagating along the density gradient and in the opposite direction have equal $|N_\xi|$ values. In this case, the dispersion dependence $N_\xi(q_e)$ can be obtained using Fig. 1. It is presented in Fig. 7. In both figures, the dispersion curve corresponding to left-handed polarized waves comes close to and touches the vertical straight line $q_e = 1$. Over the contact area, these waves should be regarded as ordinary ones (see Section 2). As the value of N_ζ grows, the point of contact shifts upwards from the q_e-axis. When N_ζ is close to $N_{\zeta,+}^{opt} = \chi\sqrt{\varepsilon_{+,c}}$, another curve corresponding to extraordinary waves undergoes deformation, apparent as a hump (Fig. 8a). If $N_\zeta = N_{\zeta,+}^{opt}$, the dispersion dependences in the vicinity of $q_e = 1$ take the form of intersecting straight lines $N_\xi = \sqrt{\varepsilon_{+,c}}$, $N_\xi = \sqrt{\varepsilon_{+,c}} + 2\delta q_e/(\chi^2\sqrt{\varepsilon_{+,c}})$ (Fig. 8b). The joining of these curves on the CS at $N_\zeta = N_{\zeta,+}^{opt} = \varepsilon_{+,c}^{1/2}\sin\chi$ suggests the possibility of complete transformation of ordinary waves into extraordinary ones (O-X transformation). A further growth of N_ζ leads to the divergence of the dependences. In this case, the point of contact with the vertical line $(q_e = 1)$ for $N_\zeta > N_{\zeta,+}^{opt}$ moves away to another dispersion curve corresponding to extraordinary waves and adjoining the vertical line on the side of $q_e > 1$ (Fig. 8c).

An enlargement of the angle χ causes a decrease in the value of $N_\xi = \varepsilon_{\sigma,c}^{1/2}\cos\chi$ at which the waves easily penetrate the CS (the dispersion curves intersect at the vertical line $q_e = 1$). The picture obtained in the limiting case of $\chi = \pi/2$ at $N_\zeta = N_{\zeta,+}^{opt}$, $N_y = 0$ is shown in Fig. 9. It is for this configuration, characteristic of closed traps, that the O-X-B

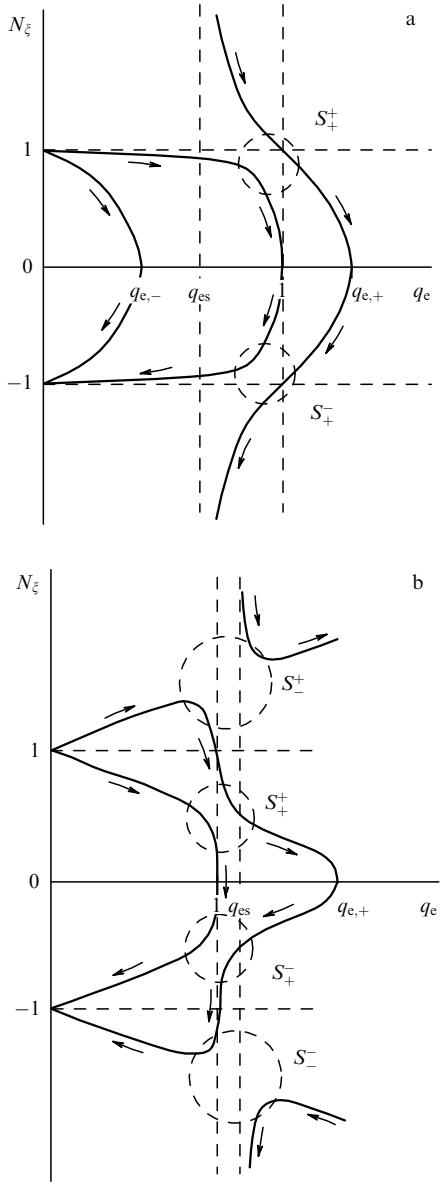

Figure 7. Dispersion dependences for waves in a plane plasma layer that propagate along the density gradient for $\chi \ll 1$. Arrows indicate directions of the energy flow; the sign denoted by the superscript on $S_\sigma^\pm$ coincides with the sign of N_ξ: (a) $\Omega_e < 1$, and (b) $\Omega_e > 1$.

transformation heating was considered in Ref. [7] (see also Section 9.2). In this scheme, the penetration of the CS by electromagnetic waves is regarded as the O-X transformation. An extraordinary wave resulting from this conversion does not penetrate very deeply behind the CS $(q_e > 1)$. After reflection from the dense plasma region, the extraordinary wave moves outside and traverses the CS without obstacle. Its refractive index as it crosses the CS takes a unit value (see Section 2). In the region with $q_e < 1$, the wave asymptotically approaches the plasma resonance surface. The growth of the refractive index in the vicinity of this surface makes effects from the thermal motion of charged particles much more significant. They promote the extension of a sequence of wave energy conversions — the extraordinary wave transforms into the Bernstein mode (X-B transformation). Generally speaking, the latter possesses no density limit. Due to this, there is a real possibility of injecting the wave energy into a plasma having a density much higher than the critical one. This

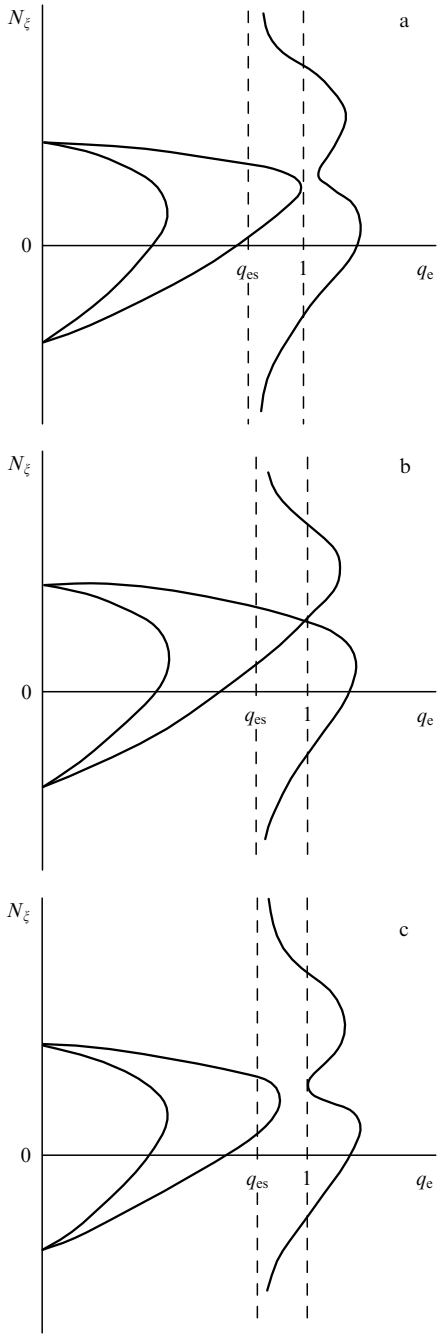

Figure 8. Dispersion dependences for waves in a plane plasma layer as $\Omega_e < 1$, $0 < \chi < \pi/2$, and $N_\zeta \approx N_{\zeta,+}^{opt}$: (a) $\delta N_\zeta < 0$, (b) $\delta N_\zeta = 0$, and (c) $\delta N_\zeta > 0$.

possibility was realized in experiments at the W7-AS stellarator [25–27].

In the case of $\omega < \omega_e$, the critical surface is reached by both the left-handed polarized and right-handed polarized (helical) waves. The dependence $N_\xi(q_e)$ for the left-handed polarized waves undergoes no significant change compared with the dependence in the case of $\omega > \omega_e$. The only difference is the following: for $\omega > \omega_e$, quasi-potential waves interacting with the left-handed polarized ones are absorbed near the plasma resonance surface; for $\omega < \omega_e$, the quasi-potential waves in the region with $q_e < 1$ are transformed into right-handed polarized ones upon removal from the CS (see Figs 7a and 7b for comparison).

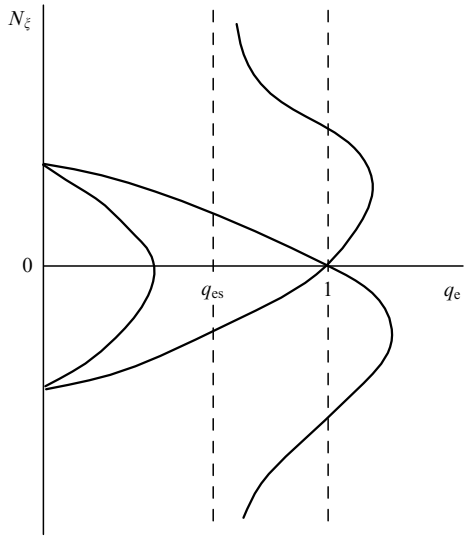

Figure 9. Dispersion dependences for waves in a plane plasma layer as $\Omega_e < 1$, $\chi = \pi/2$, and $N_\zeta = N_{\zeta,+}^{opt}$.

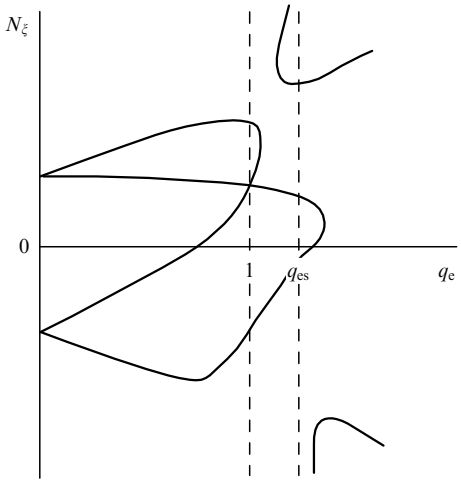

Figure 10. Dispersion dependences for waves in a plane plasma layer as $\Omega_e > 1$, and $N_\zeta = N_{\zeta,+}^{opt}$.

In the vicinity of the CS, at $N^2 \approx \varepsilon_\sigma$, the dispersion dependences are universal in character (see Figs 4–6). Therefore, when considering different values of the angle χ for $\omega_e > \omega$, we present the dispersion dependences only at the value of $N_{\zeta,c}^{opt} = \sqrt{\varepsilon_{\sigma,c}} \sin\chi$ optimal for the wave penetration through the CS.

Figure 10 illustrates characteristic dispersion dependences for oscillations with $\omega < \omega_e$ at $N_\zeta = N_{\zeta,+}^{opt}$. Figure 11 displays changes in the dispersion dependences for waves with $N_\zeta = N_{\zeta,-}^{opt}$ upon an increase in the angle χ. If the angle $\chi > \chi_{cr} = \arccos\Omega_e^{-1}$, a given constituent of the refractive index of the waves under consideration in a vacuum exceeds unity. As a result, the region of small plasma densities becomes nontransparent (Fig. 11b). A further increase in χ leads to the extension of the nontransparent region. If the angle $\chi > \chi_{max}$, the nontransparent region for right-handed polarized waves with $N_\zeta = N_{\zeta,-}^{opt}$ in the vicinity of the CS contracts to a point localized at this surface ($q_e = 1$). For waves with $N_\zeta \neq N_{\zeta,-}^{opt}$ and for $\chi > \chi_{max}$, the transparent region becomes finite, i.e., a wave channel is formed that adjoins the CS (see Section 3.1).

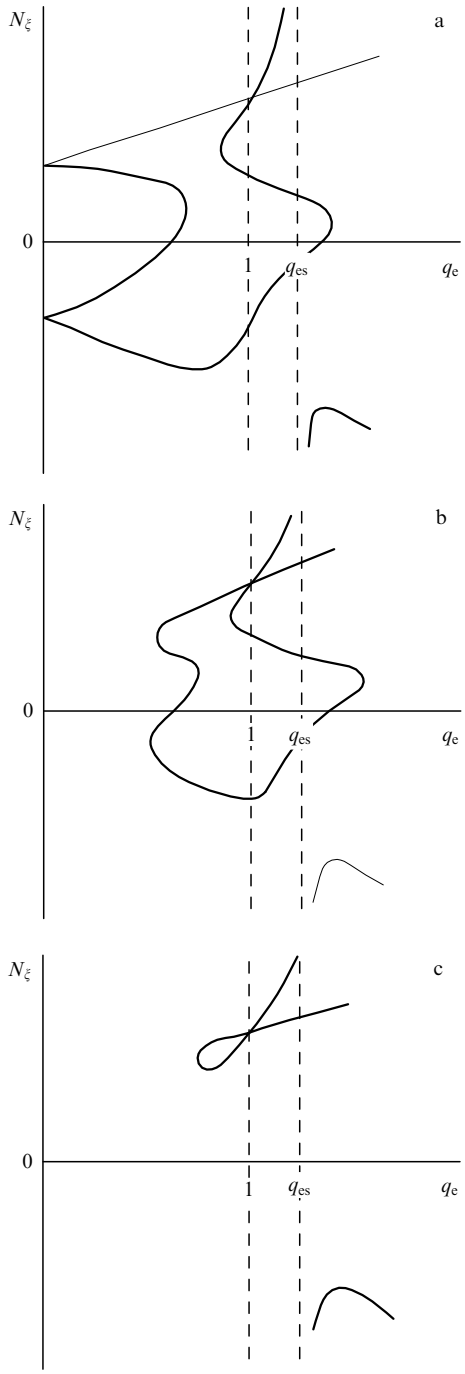

Figure 11. Dispersion dependences for waves in a plane plasma layer as $\Omega_e > 1$, and $N_\zeta = N_{\zeta,-}^{opt}$: (a) $\chi < \chi_{cr} = \arccos \Omega_e^{-1}$, (b) $\chi_{cr} < \chi < \chi_{max} = \arccos (2\Omega_e - 1)^{-1/2}$, and (c) $\chi < \chi_{max}$, $\chi \approx \chi_{max}$.

4. Transfer of electron Langmuir oscillation energy from a magnetized plasma into a vacuum

As shown in Section 3, both left and right-handed polarized waves approaching a CS can take the form of electron Langmuir oscillations. Also, it was noted that, due to the reversibility of electrodynamic equations, potential electron Langmuir oscillations traveling away from the CS must turn into electromagnetic waves. Let us find conditions under which the process in question results in the outflow of the energy of electron Langmuir oscillations into a vacuum [15]. For a plane-layered plasma, this problem may be considered using the data presented in Section 3.

It was demonstrated in Section 3.2 that for electromagnetic waves with $N_y = 0$, $N_\zeta \neq N_{\zeta,\sigma}^{opt}$ being transformed into electron Langmuir oscillations near the CS, the approximate equality $N_x^2 \approx (N_\xi \sin\chi - N_\zeta \cos\chi)^2 \approx \text{const} \cdot \xi$ is deduced. Thus, in the $q_e N_\xi$-plane, the points of contact between the dispersion curve and the vertical line $q_e = 1$ correspond to electron Langmuir oscillations. If the dispersion curve being in contact with the straight line $q_e = 1$ extends as far as the ordinate axis on which $q_e = 0$, the energy of electron Langmuir oscillations flows out into a vacuum. It follows from the discussion in Section 3 that at $N_y = 0$ the points of contact exist at any N_ζ values.

Figure 8 shows that at frequencies $\omega > \omega_e$, the vertical line $q_e = 1$ adjoins the dispersion curve for left-handed polarized (ordinary) waves with $N_\zeta < \varepsilon_{+,c}^{1/2} \sin\chi$, which have $N_\xi < \varepsilon_{+,c}^{1/2} \cos\chi$ $(N < \varepsilon_{+,c}^{1/2})$ at the CS. It is such oscillations that may pass to the vacuum. If $N_\zeta > \varepsilon_{+,c}^{1/2} \sin\chi$, the dispersion curve comes close to the vertical line $q_e = 1$ from the dense plasma side (extraordinary waves). In this dispersion curve, density varies nonmonotonically, and it again intersects the vertical line $q_e = 1$ at the unit value of the total refractive index (see Section 3.3). In the region $q_e < 1$, the dispersion curve asymptotically approaches the vertical line $q_e = q_{es}$ (plasma resonance surface). In a plane-layered plasma, the plasma resonance surface is localized at a density value given by condition (2.11). In the vicinity of the resonance surface, the waves are absorbed due to a sharp increase in the refractive index.

It should be noted that the point of contact between the dispersion curve and the vertical line $q_e = 1$ coincides at $N_\zeta = \sin\chi$ with their intersection point corresponding to the unit value of the refractive index, and the dispersion curve takes the form of a cubic parabola. At a further increase of N_ζ, the points of contact and intersection points diverge again, and the dispersion curve approaches the vertical line $q_e = 1$ at the point of contact from the lower-density side.

The picture of dispersion dependences on the $q_e N_\xi$-plane for $\omega < \omega_e$ is much more complicated because both ordinary (left-handed polarized) and extraordinary (right-handed polarized) waves can approach the CS from the low-density side (Figs 2 and 7b). The latter have $\varepsilon_{+,c}^{1/2} \sin\chi < N_\zeta < \varepsilon_{-,c}^{1/2} \sin\chi$ at the CS. Accordingly, electron Langmuir oscillations with $N_\zeta < \varepsilon_{+,c}^{1/2} \sin\chi$ escape into the vacuum via the stage of ordinary waves, and those with $\varepsilon_{+,c}^{1/2} \sin\chi < N_\zeta < \varepsilon_{-,c}^{1/2} \sin\chi$ via the stage of extraordinary waves. Waves with $N_\zeta > \varepsilon_{-,c}^{1/2} \sin\chi$ are absorbed near the plasma resonance surface.

If the frequency $\omega \to \omega_e$, the maximum value of N_ζ at which the energy of electron Langmuir oscillations can flow out into the vacuum is increased without bound. In the vacuum, however, $N = 1$ and the refractive index component N_ζ is conserved during the wave propagation over a plane-layered plasma. Therefore, only oscillations with $N_\zeta < 1$ are of interest. Also, it is worthy to note that for $\chi > \chi_{max} = \arccos (2\Omega_e - 1)^{1/2}$ the transparent region for extraordinary waves is bounded on the lower-density side — the wave channel forms near the CS (see Sections 3.1 and 5).

The mechanism of outflow of the energy of electron Langmuir oscillations into the vacuum, considered in this section, acts only in a magnetized plasma. Indeed, the weakening of the magnetic field has two consequences. First, the resonance surface at which the condition $q_{es} = (1 - \Omega_e^2)/(1 - \Omega_e^2 \cos^2\chi)$ is fulfilled comes closer to the CS. This must facilitate absorption of electron Langmuir

oscillations. Second, the entire set of values of the refractive index of waves able to emanate from the plasma to the vacuum tends to zero together with a value of $\varepsilon_{\pm,c} = [\Omega_e/(\Omega_e \pm 1)]^{1/2}$.

The outflow of the energy of electron Langmuir oscillations from a nonmagnetized plasma occurs through a different mechanism. In the absence of a magnetic field, the refractive index of electromagnetic waves equals $N^2 = \varepsilon$. In a plane-layered plasma ($\varepsilon = -\xi/L$), one finds $N_\xi^2 = -N_y^2 - \xi/L$. If the refractive index component $N_y = 0$, the electromagnetic waves come very close to the CS (reflect from the CS). Their electric field is orthogonal to the density gradient, which makes them unable to interact with electron Langmuir oscillations. Indeed, in the absence of dissipative effects in a cold plasma, electron Langmuir oscillations are localized in the plane $\xi = 0$ and have a singular electric field (see, for instance, Ref. [28]) directed along ξ.

If the refractive index component $N_y \neq 0$, *P*-polarized waves (with the magnetic field directed orthogonally to the plane of incidence) acquire the ξ-component of the electric field and may receive energy from electron Langmuir oscillations. However, this process is hampered by the necessity of traversing the nontransparent region (see, for instance, Refs [1 – 3]).

As regards *S*-polarized waves (with the direction of the electric field perpendicular to the plane of incidence), they do not interact with electron Langmuir oscillations, similar to the waves with $N_y = 0$. Thus, the outflow of the energy of electron Langmuir oscillations from a nonmagnetized plasma must be less efficient than from a magnetized plasma.

5. Wave channel near the critical surface

It was shown in Section 3 that if $\chi < \chi_{max}$, both left- and right-handed polarized waves easily penetrate a CS at $N_\zeta = N_{\zeta,\sigma}^{opt}$, $N_y = 0$. However, the transparent region for the right-handed polarized waves with 'optimal' N_ζ, N_y values is reduced on the lower-density side with increasing angle χ (see Fig. 11). For $\chi \geqslant \chi_{max}$, the transparent region degenerates into a surface congruent to the critical one. The degeneracy is removed (i.e., a wave channel is formed) if $N_\zeta \neq N_{\zeta,-}^{opt}$. The position of wave channel boundaries can be found from the condition $G > 0$ [see Eqn (3.2)]. The wave channel adjoins the CS from the lower-density side if $\delta N_\zeta < 0$, and from the higher-density side if $\delta N_\zeta > 0$ (see Fig. 6).

Let us consider in greater detail configurations with $\chi = \pi/2$, characteristic of the most popular closed magnetic traps. In this case, polarization of waves traveling through the wave channel has some peculiarities. It follows from the data considered in Section 3.2 that at $N_y = 0$ waves on the CS are transformed into electron Langmuir oscillations with $E = E_\parallel$. On the other hand, wave polarization is purely circular at the other boundary where the quantity N_x also vanishes, as on the CS, and $\delta q_e \neq 0$. Thus, the waves under consideration propagating along the wave channel as potential electron Langmuir oscillations are alternately transformed into their opposite, i.e., electromagnetic waves with transverse circular polarization, and vice versa.

Dispersion effects cause wave packet spreading along ray paths, thus resulting in the generation of natural oscillations. The spectrum of natural oscillations is determined by the relation linking quantities ω, N_y, and N_z. This relation is easiest to derive if the problem of natural oscillations is formulated as the problem of finding eigenvalues $\delta N_z = N_z - N_{z,-}^{opt}$ at fixed ω and N_y.

In a quasi-classical approximation, it is possible to use the approximate dispersion relation (3.6) which, in the given case of the plane plasma layer [$q_e(x) = 1 + x/L$], takes the form

$$N_x^2 = -N_y^2 + \frac{2\omega}{\omega_e}\left[\frac{\omega_e(\omega_e - \omega)}{\omega^2}\,\delta N_z - \left(\frac{x'}{L}\right)^2\right],$$

where

$$x' = x - \frac{\sqrt{\omega_e(\omega_e - \omega)}}{\omega}\,L\,\delta N_z\,, \qquad \delta N_z = N_z - N_{z,-}^{opt}\,.$$

The quantization condition

$$\oint \mathrm{d}x\, N_x = (2n+1)\pi$$

leads to the following spectrum of eigenvalues:

$$\delta N_z = \frac{\omega^{3/2}}{(2\omega_e\omega)^{1/2}(\omega_e - \omega)}\left[\left(\frac{\omega_e}{2\omega}\right)^{1/2} N_y^2 + \frac{2n+1}{L}\right]^{1/2}.$$

In closed traps, the plasma density is constant on nested toroidal magnetic surfaces. Due to this, the wave channel has the form of a toroidal layer near the CS. Its presence in the tokamak plasma is confirmed by numerical calculations of ray paths carried out in Ref. [17]. The ray paths computed in this work remain concentrated within a narrow region in the vicinity of the CS.

A simplified model of tokamak plasma was used in Ref. [17]. It was assumed that $\mathbf{B} = (0, B_\theta, B_\varphi)$, $B_\varphi \approx B \approx B_0 R_0/R \approx B_0[1 - (r/R_0)\cos\theta]$, and the inverse 'stability factor' $\iota = R_0 B_\theta/(rB_\varphi) = 3$, where R_0, r were the 'major' and 'minor' radii, respectively, θ was the poloidal angle, and φ was the toroidal angle. The density distribution along the minor radius was given by the dependence $q_e(r) = 3\exp[-(r/L)^2]$, where $R_0/L = 6\sqrt{5}$. Figure 12 gives an idea of typical ray paths near the CS. It depicts projections of the ray paths upon the tokamak vertical cross section (plane $\varphi = \text{const}$). The center of the Cartesian xy-coordinate system coincides with the magnetic axis.

Due to tokamak symmetry with respect to toroidal angle φ, the quantity N_φ is conserved in the ray path, whereas $N_\parallel$ becomes a function of coordinates: $N_\parallel \approx N_\varphi R_0/R$. $N_{\parallel,-}^{opt} = [\omega_e/(\omega_e - \omega)]^{1/2}$, together with the magnetic field, equally depends on the coordinates. Within a given magnetic surface with which the CS is associated, $N_\parallel$ takes a maximum value on the inside of the torus ($\theta = \pi$), and $N_{\parallel,-}^{opt}$ on the outside of the torus ($\theta = 0$). The transparent region (wave channel) in tokamaks, as in other closed traps, has the form of a narrow toroidal layer. The results presented in Section 3.1 indicate that in the transparent region the condition $q_e > 1$ must be satisfied for oscillations with $N_\parallel > N_{\parallel,-}^{opt}$, and the condition $q_e < 1$ for waves with $N_\parallel < N_{\parallel,-}^{opt}$. Therefore, if the waves with $N_\parallel$ slightly larger than $N_{\parallel,-}^{opt}$ are launched from the inner side of the torus they must be reflected, when propagating along the magnetic surface, from the region in which $N_\parallel$ becomes approximately equal to $N_{\parallel,-}^{opt}$. Definite precise adjustment of the initial conditions would be needed to ensure the penetration of these waves through the CS into the region where $q_e < 1$. Thus, it can be concluded that the oscillations with $N_\parallel$ slightly in excess of $N_{\parallel,-}^{opt}$ must be localized on the inner side of the torus. A similar line of reasoning indicates that oscillations with $N_\parallel$ slightly smaller

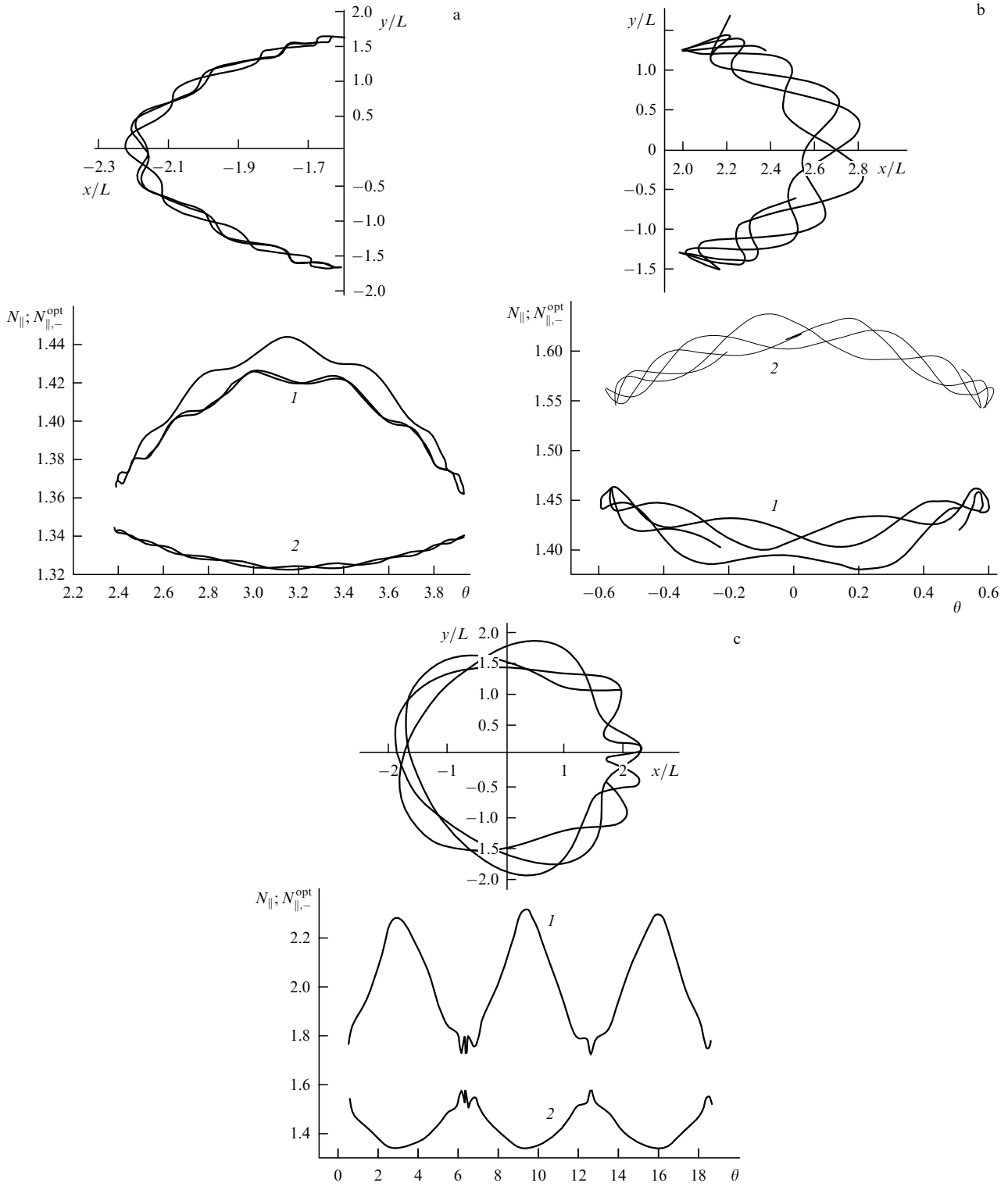

Figure 12. Ray paths (projections onto the vertical plane along the circumferences of the major radius) of electromagnetic waves in a tokamak plasma near the CS and dependences of $N_\parallel$ (curves *1*) and $N_{\parallel,-}^{\rm opt}$ (curves *2*) on the poloidal angle in the ray paths: (a) $N_\parallel > N_{\parallel,-}^{\rm opt}$, (b) $N_\parallel < N_{\parallel,-}^{\rm opt}$, (c) marked excess of $N_\parallel$ over $N_{\parallel,-}^{\rm opt}$.

than $N_{\parallel,-}^{\rm opt}$ are localized on the outer side of the torus. At the same time, when there is a large difference between $N_\parallel$ and $N_{\parallel,-}^{\rm opt}$, the ray paths wind around the full length of the torus (Fig. 12c).

A nonequilibrium plasma may contain, for example, electron beams traveling along the magnetic field or display anisotropic electron velocity distribution as is frequently the case with the electron cyclotron resonance (ECR) heating. In this situation the waves under consideration may lose stability and have a very large amplitude.

In open traps, the angle χ varies from $\chi = \pi/2$ in the median plane to $\chi = 0$ on the axis. With the motion along the CS from a given plane towards the magnetic mirrors, the angle χ decreases. This causes the channel to broaden. When

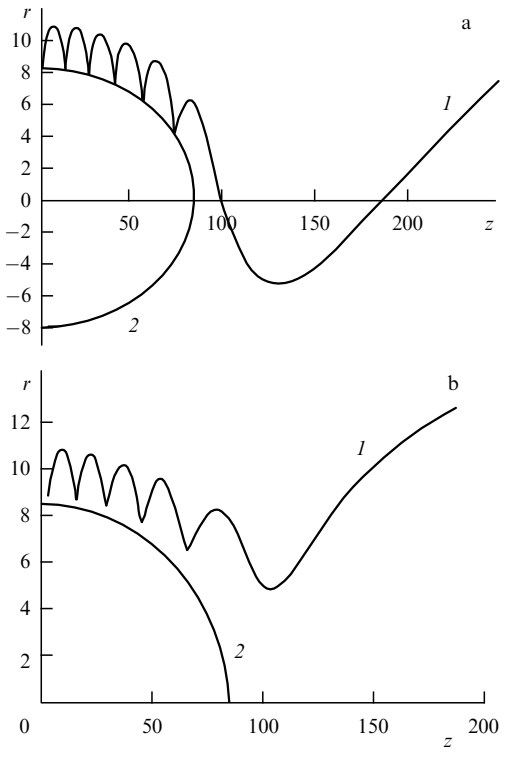

Figure 13. Ray paths of electromagnetic waves in an open-trap plasma near the CS: (a) $N_\varphi = 0$, (b) $N_\varphi = 0.2 \sin 0.75$; *1* — ray path, *2* — CS.

the angle χ exceeds the value of $\chi_{\max}$ given by condition (3.4), the channel 'opens' and, in the thin-layer approximation applied in Section 3, its width goes to infinity. This means that electromagnetic waves can leave the CS and pass to the vacuum.

The phenomenon of wave channel opening was illustrated by calculations of the ray paths done for the plasma in an open magnetic trap in Ref. [14]. In this calculations, the magnetic field was given by the potential

$$\Phi(\mathbf{r}) = \Phi_0(z) - \frac{r^2}{4}\,\Phi_0''(z)\,,$$

where

$$\Phi_0(z) = \frac{1}{2}\left[(R+1)z - (R-1)\,\frac{L_B}{\pi}\sin\left(\pi\,\frac{z}{L_B}\right)\right],$$

$$R = 2\,, \qquad L_B = 200\,.$$

A cylindrical coordinate system having the Z-axis coincident with the trap axis was used in computation. It was assumed that the plasma slab has the shape of an axially extended ellipsoid:

$$q_\mathrm{e}(\mathbf{r}) = q_\mathrm{e}(0)\exp\left[-\left(\frac{r}{L_r}\right)^2 - \left(\frac{z}{L_z}\right)^2\right],$$

$$L_r = 10\,, \qquad L_z = 100\,, \qquad q_\mathrm{e}(0) = 2\,, \qquad \Omega_\mathrm{e}(0) = 2\,.$$

Examples of ray paths localized on the outer side of the CS are presented in Fig. 13. Both paths originate from the same point ($r = 10$, $z = 0.1$) and at equal values of $N_\perp = 0.2$ However, in the second case, the angle of wave vector deflection from the zr-plane is equal to 0.75 ($N_\varphi \neq 0$). The two ray paths oscillate along the radius in the vicinity of the median surface but monotonically move away from the axis as they approach the magnetic mirrors. This suggests an 'opening' of the wave channel. It follows from the results presented in Section 3 that, if $N_\varphi \neq 0$, an oscillating ray path does not reach the CS. Outside the trap, i.e., in the low-density region, the 'centrifugal force' repels such a ray from the system's axis. The value of $N_\parallel$ on both paths varies only insignificantly: from $N_\parallel \approx 1.25$ inside the plasma to $N_\parallel \approx 1$ outside it. Projection of the wave phase velocity onto the magnetic field direction being below the speed of light, the Cherenkov interaction is possible between the waves under consideration and beams of charged particles traveling parallel to the magnetic field.

6. Coefficients of transmission of electromagnetic waves through the critical surface and reflections from it

6.1 General case

The analysis in Section 3 has demonstrated the presence of a nontransparent plasma region in the vicinity of a CS. In a quasi-classical approximation, the coefficient of transmission through a nontransparent region ($\xi_1 < \xi < \xi_2$) is given by the expression

$$T = \exp(-2\gamma)\,, \tag{6.1}$$

where

$$\gamma = \int_{\xi_1}^{\xi_2} \mathrm{d}\xi\ \mathrm{Im}\, N_\xi(\xi)\,. \tag{6.2}$$

In this case, the reflection coefficient equals

$$R = 1 - T\,. \tag{6.3}$$

Determination of δN_ξ from Eqn (3.1) yields [8 – 10, 24]

$$\gamma = \frac{\pi L}{2\sqrt{2}}\left(\frac{\Omega_\mathrm{e}}{g_\sigma(\Omega_\mathrm{e},\chi)}\right)^{1/2}\left(\frac{2\delta N_\zeta^2(\sigma+\Omega_\mathrm{e})}{g_\sigma(\Omega_\mathrm{e},\chi)} + N_y^2\right). \tag{6.4}$$

Expression (6.4) indicates, in particular, that the vicinity of the CS becomes nontransparent for right-handed polarized waves ($\gamma \to \infty$) when the angle χ tends to the limiting value given by condition (3.4)

The quasi-classical approximation frequently yields results that remain true beyond the validity range of the model. In particular, it holds true for the problem of wave passage through the CS. An approximate wave equation describing this process can be derived from the system of algebraic equations (2.8). As in the preceding sections, we confine ourselves to the consideration of oscillations with $N^2 \approx \varepsilon_\sigma$ that can easily penetrate through the nontransparent region in the vicinity of the CS. Let us take $N_\xi = \sqrt{\varepsilon_{\sigma,\mathrm{c}}}\cos\chi + \delta N_\xi$, $N_\zeta = \sqrt{\varepsilon_{\sigma,\mathrm{c}}}\sin\chi + \delta N_\zeta$, assume the linear dependence ($q_\mathrm{e} = 1 + \xi/L$) of the density on the ξ coordinate, and substitute $\delta N_\xi \to -\mathrm{i}\partial/\partial\xi$. This will lead to the system of equations

$$\begin{aligned}
\frac{\mathrm{d}E_\parallel}{\mathrm{d}\xi_1} &= (B + \mathrm{i}H)E_\parallel - (\sigma\xi_1 + A)F\,,\\
\frac{\mathrm{d}F}{\mathrm{d}\xi_1} &= -B^*F + \xi_1 E_\parallel\,,
\end{aligned} \tag{6.5}$$

where the following designations are used:

$$\xi_1 = (L\sin\chi)^{-1/2}\left(\frac{2}{\Omega_e}\right)^{1/4}\xi\,, \qquad F = -\mathrm{i}(\Omega_e+\sigma)^{-1/2}E_\sigma\,,$$

$$A = \frac{2^{5/4}L^{1/2}}{\sin^{3/2}\chi}\,\Omega_e^{1/4}(\Omega_e+\sigma)^{1/2}(\delta N_\zeta + \mathrm{i}N_y\cos\chi)\,,$$

$$B = \left(\frac{L}{\sin\chi}\right)^{1/2}\left(\frac{\Omega_e}{2}\right)^{1/4}(N_y - \mathrm{i}\delta N_\zeta\sin\chi)\,,$$

$$H = 2^{3/2}(\Omega_e+\sigma)^{1/2}\cot\chi\,.$$

Following Zharov [8], we introduce a new unknown function Y through which quantities F and $E_\parallel$ are expressed by the relations

$$F = (Y'_{\xi_1} + \alpha Y)\exp\left(\frac{\delta\xi_1^2}{2}\right),$$

$$E_\parallel = (\beta Y'_{\xi_1} + \nu Y)\exp\left(\frac{\delta\xi_1^2}{2}\right).$$

Constants $\alpha = -B$, $\beta_\pm = \mathrm{i}(H \pm \sqrt{H^2+4\sigma})/2$, $\nu = \beta_+B^* - A$, and $\delta = \beta_-$ are derived from the condition of identity of two equations in system (6.5), taking the form

$$Y''_{\xi_1\xi_1} - \mathrm{i}(a+b\xi_1)Y'_{\xi_1} + (c+d\xi_1)Y = 0\,, \tag{6.6}$$

where

$$a = -2\mathrm{i}\,\mathrm{Im}\,B\,, \qquad b = \mathrm{i}(-\beta_+ + \beta_-)\,,$$
$$c = -|B|^2\,, \qquad d = A - (\beta_+B^* + \beta_-B)\,.$$

By means of the substitutions

$$Y = \exp\left[\mathrm{i}\left(\frac{a}{2}\,\xi_1 + \frac{b}{4}\,\xi_1^2\right)\right]y\,,$$

$$\eta = \left(\frac{b}{2}\right)^{1/2}\xi_1 + \left(\frac{2}{b}\right)^{1/2}\left(\frac{a}{2}+\frac{d}{b}\right)$$

equation (6.6) is reduced to the standard parabolic cylinder equation [29]

$$y''_{\eta\eta} + \left(\eta^2 - \frac{2\gamma}{\pi} + \mathrm{i}\right)y = 0\,, \tag{6.7}$$

where the designation was used:

$$\gamma = \frac{\pi}{|b|}\left(\frac{d(d+ab)}{b^2} - c\right).$$

The linearly independent solutions of Eqn (6.7) have the form

$$y = D_{\mathrm{i}\gamma/\pi}\left[\pm\sqrt{2}\,\exp\left(\frac{\mathrm{i}\pi}{4}\right)\eta\right]. \tag{6.8}$$

In the region $\eta \gg 1$, $y \propto \exp(\pm\mathrm{i}\eta^2/2)$; accordingly, one obtains

$$E_\sigma, E_\parallel \propto \exp\left[\frac{\mathrm{i}}{2}\left(H \pm \sqrt{H^2+4\sigma}\right)\xi_1^2\right].$$

In order to relate these asymptotics to waves incident upon the critical surface and escaping from it, the following expression for the group velocity needs to be analyzed:

$$\frac{\mathrm{d}\omega}{\mathrm{d}N_\xi} = -\frac{\partial D/\partial N_\xi}{\partial D/\partial\omega}\,, \tag{6.9}$$

where D is the left-hand side of dispersion relation (3.1).

Using Eqn (3.1), it is found that the sign of the quantity $\partial D/\partial\omega$ entering the expression for group velocity is congruent to the sign of δq_e:

$$\omega\,\frac{\partial D}{\partial\omega} = \frac{2+3\sigma\Omega_e+2\Omega_e^2}{(1+\sigma\Omega_e)^2}\,\delta q_e + \frac{\Omega_e}{\Omega_e+\sigma}\,\frac{N_\perp^2}{\delta q_e}\,. \tag{6.10}$$

It should be recalled that only left-handed polarized waves ($\sigma = +1$) can approach the CS for $\Omega_e < 1$.

The following equation is obtained for the quantity $\partial D/\partial N_\xi$:

$$\frac{\partial D}{\partial N_\xi} = \pm G^{1/2}\,, \tag{6.11}$$

where the discriminant G of the quadratic equation is given by formula (3.2).

The plus sign in Eqn (6.11) corresponds to the root of equation (3.1) with a larger modulus in the region behind the CS ($q_e > 1$), and to the root with a smaller modulus in front of it ($q_e < 1$). The reverse position of roots in relation to the CS is true for the minus sign. It was noted in the analysis of Eqn (3.1) in Section 3 that, in the case of $\chi \ll 1$, the root with a larger modulus corresponds to quasi-potential waves, and that with a smaller modulus to circularly polarized waves. Because we consider waves with $N_\xi > 0$ (for definiteness) and $N_\xi \gg |\delta N_\xi|$, it is concluded that, in this case, the dispersion is normal for circularly polarized waves (projections of group and phase velocities onto the ξ-axis have identical signs), and abnormal for quasi-potential waves. In Fig. 7, the direction of group velocity is shown by the arrows.

In the region behind the CS ($q_e > 1$), waves propagating to the right are described by the following solution to Eqn (6.7):

$$y = D_{\mathrm{i}\gamma/\pi}\left[-\sqrt{2}\,\exp\left(\frac{\mathrm{i}\pi}{4}\right)\eta\right]$$
$$\underset{\eta\to-\infty}{\approx} (\sqrt{2}\,\eta)^{\mathrm{i}\gamma/\pi}\exp\left(-\frac{\gamma}{4}\right)\exp\left(-\frac{\mathrm{i}\eta^2}{2}\right). \tag{6.12}$$

This solution in the front region of the CS has the asymptotics

$$y \underset{\eta\to-\infty}{\approx} (\sqrt{2}\,\eta)^{\mathrm{i}\gamma/\pi}\exp\left(-\frac{\gamma}{4}\right)\exp\left(-\frac{\mathrm{i}\eta^2}{2}\right)$$
$$-\frac{\sqrt{2\pi}}{\Gamma(-\mathrm{i}\gamma/\pi)}\exp\left(-\frac{3\gamma}{4}\right)(\sqrt{2}\,\eta)^{-\mathrm{i}\gamma/\pi-1}\exp\left(\frac{\mathrm{i}\eta^2}{2}\right). \tag{6.13}$$

Comparison of the first term in formula (6.13) with expression (6.12) gives transmission coefficient (6.1). When determining the reflection coefficient, it should be taken into account that asymptotics of incident and reflected waves are differently expressed via the function Y. Specifically, for an incident wave, one finds

$$F \approx \left(-\mathrm{i}\,\frac{d}{b} + \alpha\right)\exp\left(\frac{\mathrm{i}\delta\xi_1^2}{2}\right)Y\,,$$

$$E_\parallel \approx \left(-\mathrm{i}\beta\,\frac{d}{b} + \nu\right)\exp\left(\frac{\mathrm{i}\delta\xi_1^2}{2}\right)Y\,,$$

while for a reflected wave, the result is as follows

$$F \approx \mathrm{i}b\xi_1 \exp\left(\frac{\mathrm{i}\delta\xi_1^2}{2}\right) Y\,, \qquad E_\parallel \approx \mathrm{i}b\beta\xi_1 \exp\left(\frac{\mathrm{i}\delta\xi_1^2}{2}\right) Y\,.$$

Also taking into consideration the relation [29]

$$\frac{1}{\left|\Gamma(-\mathrm{i}\gamma)\right|^2} = \frac{\gamma}{\pi}\sinh(\pi\gamma)\,,$$

it is found that the reflection coefficient is given by relationship (6.3), in accordance with the law of conservation of energy. Certainly, the same relations (6.1) – (6.4) characterize waves incident upon the CS from the higher-density side.

Partial reflection of waves incident upon the CS can result in a trebling of a radio signal reflected from the earth's magnetosphere (see Refs [1 – 3, 6]). The atmospheric gas begins to be ionized at a certain altitude above the earth's surface and plasma density increases to a threshold value with distance from the surface. Hence, the dispersion dependences illustrated by Figs 1 and 2 (see also Section 6.2) give a general idea of the propagation of radio waves emitted from terrestrial sources.

A nonpolarized radio signal in a magnetic field splits into two components corresponding to ordinary (left-handed polarized) and extraordinary (right-handed polarized) waves, respectively. Hence, there must be two reflected signals separated in time. However, if a radio signal approaching the CS has small values of $\delta N_\zeta = N_\zeta - N_{\zeta,\sigma}^{\mathrm{opt}}$ and N_y, only part of the right-handed polarized waves are reflected from this surface, and a certain amount of electromagnetic energy is transferred through it. The geometry of the magnetosphere is distinct from that of a plane layer. Therefore, generally speaking, waves that penetrate the CS and are then reflected from the dense plasma can hardly come back to the same surface at an angle enabling them to return to the earth. However, if the magnetic field incorporates inhomogeneities, scattering from them may result in the outflow of a fraction of wave energy. Due to this, the third reflected signal may appear in the case of $\Omega_\mathrm{e} < 1$. When $\Omega_\mathrm{e} > 1$, the picture of dispersion dependences becomes even more complicated and the number of reflected signals can be as large as seven [1].

6.2 Small angle between the plasma density gradient and magnetic field vector

The dispersion curves come closest to each other (and intersect at $N_\zeta = N_{\zeta,\sigma}^{\mathrm{opt}}$) in the regions designated as $S_\sigma^\pm$ in Figs 8a and 10a (superscript '$\pm$' on $S_\sigma^\pm$ corresponds to the sign of N_ξ unrelated to the sign of wave polarization denoted by the subscript). In these regions, the wave energy 'flows' from one dispersion curve to another, which leads to a change in polarization of waves and to their absorption if the respective dispersion curve has vertical asymptote $q_\mathrm{e} = q_\mathrm{es}$ (plasma resonance). For short (quasi-classical) waves, the 'flow' is characterized by coefficients of transmission (6.1) and reflection (6.3).

The wave energy transferred through the nontransparent region must travel away from its border. The signs of group velocity need to be found in order to know along which dispersion curve in the $q_\mathrm{e}N_\xi$-plane the wave energy will be 'flow'. The directions of group and phase velocities coincide far from the critical surface, where the dispersion relations for electromagnetic waves have the form $N^2 \approx \varepsilon_\sigma$. Generally speaking, this peculiarity is sufficient to obtain a complete picture of wave propagation in the $q_\mathrm{e}N_\xi$-plane while accounting for the continuity of the wave energy flow. This picture is represented in Fig. 7 where the arrows indicate directions of the wave energy flow.

In addition, this picture is warranted by the results of the direct group-velocity computation for another limiting case of quasi-potential waves close to the plasma resonance state. Waves in a cold plasma become potential when $N \to \infty$. The dispersion relation for such waves, which is equivalent to Eqn (2.5), is bilinear in the refractive index:

$$D = N_i N_k \varepsilon_{ik} = 0\,. \tag{6.14}$$

The use of this relation helps to find the group velocity

$$V_i = -\frac{\partial D/\partial N_i}{\partial D/\partial\omega} \propto N_k \varepsilon_{ik}\,. \tag{6.15}$$

Expression (6.15) shows that the group velocity for the potential waves is orthogonal to the vector **N** [30]:

$$N_i V_i \propto N_i N_k \varepsilon_{ik} = 0\,. \tag{6.16}$$

In the vicinity of the plasma resonance surface, the passage to the limit occurs: $N_\xi \to \infty$ (see Section 3.1) and, accordingly, $V_\xi \to 0$. Therefore, the finiteness of the N_ζ/N_ξ ratio needs to be taken into consideration in order to find V_ξ. Representation of relation (6.14) for $\chi \ll 1$ in the form

$$(\chi N_\xi - N_\zeta)^2 \varepsilon_\perp + N_\xi^2 \varepsilon_\parallel = 0 \tag{6.17}$$

leads to the desired result:

$$V_\xi \approx -\frac{\omega\chi\varepsilon_\perp N_\zeta}{N_\xi^2}\,. \tag{6.18}$$

Expression (6.18) holds true near the plasma resonance surface.

The group velocity in the vicinity of the CS at values of the angle χ close to unity was computed in Section 6.1. All these findings are in agreement with the wave energy transportation pattern depicted in Fig. 7.

Based on this picture, we shall first consider a simpler case of $\omega > \omega_\mathrm{e}$, when only left-handed polarized waves can reach the CS. Let a unit wave energy flux be incident on the CS from the lower-density side. In the region of S_+^+, the part of this flux, equalling T_+^+ (here, the subscript characterizes polarization of oscillations $\sigma = +$, and the superscript denotes the sign of N_ξ), will pass through the CS and propagate behind it in the same direction in the form of left-handed polarized electromagnetic waves. Part of the energy (equal to $1 - T_+^+$) that penetrates the CS remains on the steeply descending portion of the initial dispersion curve, corresponding to quasi-potential waves that resemble electron Langmuir oscillations. In the interaction region S_+^-, the part of the energy [equal to $(1 - T_+^+)\,T_+^-$] is brought into the dispersion curve that goes to the plasma resonance region. It is eventually absorbed, while the remaining part $(1 - T_+^+)(1 - T_+^-)$ moves along the initial dispersion curves and takes the form of reflected left-handed polarized electromagnetic waves. Thus, transmission, reflection, and absorption coefficients of left-handed polarized waves incident upon the CS from the lower-density side are given by the

expressions

$$T_+^{\uparrow} = T_+^+ ,$$
$$R_+^{\uparrow} = (1 - T_+^+)(1 - T_+^-) , \qquad (6.19)$$
$$A_+^{\uparrow} = (1 - T_+^+)\, T_+^- .$$

When such waves are incident on the CS from the higher-density side, as shown in Fig. 7, oscillations fail to be reflected (see region S_+^+). At the same time, for the transmission and absorption coefficients we obtain

$$T_+^{\downarrow} = T_+^- , \qquad (6.20)$$
$$A_+^{\downarrow} = 1 - T_+^- .$$

In these coefficients, the up- and down-pointing arrows indicate wave propagation along the directions of increasing and decreasing plasma density, respectively.

The picture of phenomena taking place near the CS for $\omega < \omega_e$ becomes even more complicated because of a possible change in the direction of rotation of the electric field vector. By consecutively applying relationships (6.1) and (6.3) to each of the $S_\sigma^\pm$ regions through which the wave energy is transferred in accordance with Fig. 7b, it is possible to derive expressions for the coefficients that characterize wave–plasma interactions near the CS in this case, too. For the frequencies $\omega < \omega_e$, polarization of transmitted and reflected waves may alter. This polarization is indicated by the second subscript on the respective coefficients listed below.

Right-handed polarized waves incident from the lower-density side are the following:

$$T_{-,-}^{\uparrow} = T_-^+ ,$$
$$T_{-,+}^{\uparrow} = (1 - T_-^+)(1 - T_+^+) ,$$
$$R_{-,+}^{\uparrow} = (1 - T_-^+)\, T_+^+ (1 - T_+^-) , \qquad (6.21)$$
$$R_{-,-}^{\uparrow} = (1 - T_-^+)\, T_+^+ T_+^- (1 - T_-^-) ,$$
$$A_-^{\uparrow} = (1 - T_-^+)\, T_+^+ T_+^- T_-^- .$$

Left-handed polarized waves incident from the lower-density side are

$$T_{+,+}^{\uparrow} = T_+^+ ,$$
$$R_{+,+}^{\uparrow} = (1 - T_+^+)(1 - T_+^-) , \qquad (6.22)$$
$$R_{+,-}^{\uparrow} = (1 - T_+^+)\, T_+^- (1 - T_-^-) ,$$
$$A_+^{\uparrow} = (1 - T_-^+)\, T_+^- T_-^- .$$

Left-handed polarized waves incident from the higher-density side are

$$T_{+,+}^{\downarrow} = T_+^- ,$$
$$R_{+,-}^{\downarrow} = (1 - T_+^-)(1 - T_-^-) , \qquad (6.23)$$
$$A_+^{\downarrow} = (1 - T_+^-)\, T_-^- .$$

Right-handed polarized waves incident from the higher-density side are

$$T_{-,-}^{\downarrow} = T_-^- , \qquad (6.24)$$
$$A_-^{\downarrow} = 1 - T_-^- .$$

The remaining coefficients ($T_{+,-}^{\uparrow}$, $R_{+,+}^{\downarrow}$, $R_{+,-}^{\downarrow}$, $T_{-,+}^{\downarrow}$, $R_{-,+}^{\downarrow}$, $R_{-,-}^{\downarrow}$) vanish.

Coefficients $T_\sigma^\pm$ characterize the passage of waves through one of the interaction regions $S_\sigma^\pm$. These coefficients were presented in Section 6.1. It should be noted that the superscript on the coefficients $T_\sigma^\pm$ enters the expression $\delta N_\zeta^\pm = N_\zeta \mp \sin\chi\sqrt{\varepsilon_\sigma}$ [see Eqns (6.1)–(6.4)].

The computation of coefficients $T_\sigma^\pm$ in the case of $\chi \ll 1$ can be significantly simplified. It follows from relation (3.3) that a decrease of angle χ reduces the size of the interaction (nontransparent) region: $\delta q_{e,1} \propto \sin\chi$. Within this region, the quantities ε_σ, $\varepsilon_\perp$ may be regarded as constants for $\chi \ll 1$, as in the derivation of relationship (3.10), with account for the coordinate dependence in the expression for $\varepsilon_\parallel = -\delta q_e = -\xi/L$ alone. In this case, the term $\propto \delta q_e^2$ is lost in the dispersion relation (3.1) and coefficients of the respective wave equation retain only the linear coordinate dependence. The wave equation is obtained, as in Section 6.1, by means of the substitution $\delta N_\xi \to -\mathrm{i}\partial/\partial\xi$. It ensues from the original system of equations (2.8) that the resultant operator must be applied to $E_\parallel(\xi)$:

$$\left\{\chi^2 \frac{\partial^2}{\partial\xi^2} + 2\mathrm{i}\,\frac{\partial}{\partial\xi}\left(\frac{2\xi}{L\varepsilon_{\sigma,c}^{1/2}} + \chi\,\delta N_\zeta\right) - (\delta N_\zeta)^2 - N_y^2\right\} E_\parallel = 0 . \qquad (6.25)$$

By virtue of the linear coordinate dependence of the coefficients of this equation, it is convenient to solve it by the complex Fourier transform method (see Appendix 1). Analysis of the solutions confirms the validity of the expressions (6.1) and (6.3) for transmission and reflection coefficients, respectively.

Coefficients (6.18)–(6.23) were obtained by the consecutive application of relationships (6.1)–(6.3) that characterize the wave passage through the interaction regions $S_\sigma^\pm$. Meanwhile, a more straightforward approach is feasible for $\chi \ll 1$, in which a unified wave equation is used that takes into consideration the entire sequence of processes proceeding in the vicinity of both the CS and the plasma resonance surface. Such an equation is derived by means of the substitution $N_\xi \to -\mathrm{i}\partial/\partial\xi$ in the dispersion relation (3.9):

$$\left\{\left(\frac{\partial^2}{\partial\xi^2} + \varepsilon_{+,c}\right)\left(\frac{\partial^2}{\partial\xi^2} + \varepsilon_{-,c}\right)\xi - \varepsilon_{\perp,c}\, L\left[\left(\chi\,\frac{\partial}{\partial\xi} - \mathrm{i}N_\zeta\right)^2 - N_y^2\right]\left(\frac{\partial^2}{\partial\xi^2} + 1\right)\right\} E_\parallel = 0 . \qquad (6.26)$$

Equation (6.26) is a singular one. The peculiarity at the point $\xi_s = \varepsilon_{\perp,c}\, L\chi^2$ corresponds to the plasma resonance. The position of this point is given by Eqn (2.5) in which $\theta = \chi$ should be set (see Section 3.3). To continue the solution through this point, we use the by-pass rule proposed by Landau that effectively takes into account the dissipation in the vicinity of the resonant point. In accordance with the general recipe, a minor positive imaginary part is added to the frequency in the equation $\varepsilon_\parallel(\omega, \xi) + \varepsilon_\perp\chi^2 = 0$ that defines the location of the singular point. Because in this case $\mathrm{d}\omega_{pe}^2/\mathrm{d}\xi > 0$, the singular point shifts in the complex plane upward from the real axis. It means that in the generalization of the solution to complex values, the singular point must be by-passed from below. Analysis of the solutions obtained with the aid of the Landau rule confirms the foregoing results (see Appendix 2).

It is worth noting that expressions (6.20) and (6.24) are similar to the known Budden coefficients that characterize

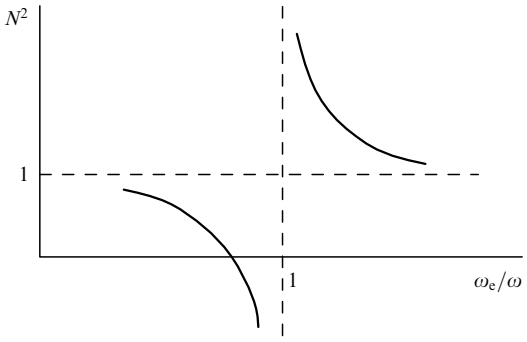

Figure 14. Refractive index of right-handed polarized waves propagating along a nonuniform magnetic field near the ECR point.

resonant interactions between electromagnetic waves incident upon the region of cyclotron resonant interaction from the higher-magnetic-field side (magnetic beach configuration) (see, for instance, Ref. [18]). These are right-handed polarized waves and their refractive index is given by the expression

$$N^2 = 1 - \frac{\omega_{pe}^2}{\omega(\omega - \omega_e)} .$$

The wavelength decreases upon approaching the cyclotron resonance point, which accounts for an intense absorption of the waves and the absence of their reflection. The passage of waves through the nontransparent region in the vicinity of the cyclotron resonance point, as in the case under consideration, is due to tunnel transition (see formula (6.1) and Refs [1, 4, 5]). The coordinate dependence of the refractive index in the vicinity of the cyclotron resonance point is presented in Fig. 14. In the case of circularly polarized waves incident upon the CS, the absorption is due to the plasma resonance (see vertical asymptotes of the dispersion dependences in Figs 1, 2, and 7).

The processes associated with the incidence of electromagnetic waves on the CS are more complex by virtue of their asymmetry with respect to the sign of N_ξ. If $\Omega_e > 1$, the picture is further complicated by the presence of two wave branches that may propagate near the CS. For $\Omega_e < 1$, only left-handed polarized waves manifest themselves in the vicinity of the CS. In the case of unessential asymmetry, when $T_+^+ = T_+^-$, coefficients (6.19) characterizing the transmission of left-handed polarized waves through the CS as they come from the lower-density side are also similar in form with the Budden coefficients.

7. Ray paths near the critical surface

In the preceding sections we have considered plane waves. As a rule, their length is small compared with the characteristic spatial scale of the plasma. Such waves are usually fed to the plasma in the form of transversely restricted wave beams. The paths of the beams can be found in the geometric optics approximation.

The system of geometric optics equations has the form

$$\begin{aligned} \dot{\mathbf{r}} &= -\frac{\partial D}{\partial \mathbf{N}} \left(\frac{\partial D}{\partial \omega}\right)^{-1} , \\ \dot{\mathbf{N}} &= \frac{\partial D}{\partial \mathbf{r}} \left(\frac{\partial D}{\partial \omega}\right)^{-1} . \end{aligned} \tag{7.1}$$

Since we are interested in the shape of ray paths alone, time t may be replaced by any other quantity t' characterizing distance along the path. Defining the new 'time' t' by the relation $\mathrm{d}t'/\mathrm{d}t = \partial D\big(\mathbf{r}(t), \mathbf{N}(t)\big)/\partial\omega$, the system of equations (7.1) is simplified and takes the form

$$\begin{aligned} \dot{\mathbf{r}} &= -\frac{\partial D}{\partial \mathbf{N}} , \\ \dot{\mathbf{N}} &= \frac{\partial D}{\partial \mathbf{r}} . \end{aligned} \tag{7.2}$$

The refractive index in the vicinity of CS is a sharply varying function of density (see Sections 2 and 5). Therefore, especially strong refraction of waves and the appearance of peculiarities in the ray paths should be expected in the given region. These peculiarities are most clearly manifest in the ray paths lying in the $\xi 0 \zeta$-plane ($N_y = 0$).

Taking advantage of the free choice of a concrete representation of the dispersion relation, it can be written down in the form

$$\delta N_\xi - F(\xi, \delta N_\zeta) = 0 . \tag{7.3}$$

Here, the function $F(\xi, \delta N_\zeta)$ is given by relations (3.1),(3.2):

$$F(\xi, \delta N_\zeta) = \frac{2\delta q_e \varepsilon_{\sigma,c}^{-1/2} \cos\chi + \delta N_\zeta \cos\chi \sin\chi \pm G^{1/2}(\xi, \delta N_\zeta)}{\sin^2\chi} , \tag{7.4}$$

where $\delta q_e = \xi/L$.

It follows from formula (7.4) that the ray path equation on the $\xi\zeta$-plane in the vicinity of CS takes the form

$$\frac{\mathrm{d}\zeta}{\mathrm{d}\xi} = -\frac{\partial F}{\partial(\delta N_\zeta)} = -\cot\chi \pm \frac{2\xi}{L\varepsilon_{\sigma,c}^{1/2} G^{1/2}(\xi, \delta N_\zeta) \sin\chi} . \tag{7.5}$$

The ray path at $N_y = 0$ can immediately adjoin the CS. Close to it ($\delta q_e \ll \delta N_\zeta$), Eqn (7.5) leads to

$$\zeta \approx -\xi\cot\chi \pm \frac{2}{3}\left(\frac{\xi^3}{L\sqrt{\varepsilon_{\sigma,c}}\,\delta N_\zeta \sin^3\chi}\right)^{1/2} . \tag{7.6}$$

It should be emphasized that the transparent region borders the CS on the higher-density side ($\xi > 0$) as $\delta N_\zeta > 0$, and on the lower-density side ($\xi < 0$) as $\delta N_\zeta < 0$; thus, the sign of ξ is coincided with the sign of δN_ζ in this region. Taking into consideration relations $z = \xi\cos\chi + \zeta\sin\chi$, $\xi = x\sin\chi + z\cos\chi$, the expression (7.6) is reduced to

$$z = \pm\frac{2}{3}\sin\chi\left(\frac{x^3}{L\sqrt{\varepsilon_{\sigma,c}}\,\delta N_z}\right)^{1/2} . \tag{7.7}$$

Expression (7.7) indicates that ray paths display cusps (Spitzen) as they approach the CS; moreover, they approach the CS and retreat from it transversely to the magnetic field (Fig. 15) (see also Refs [1, 4, 5]). This peculiarity is related to the transformation of electromagnetic waves into electron Langmuir oscillations with $N_\perp = 0$ at the CS. In a cold plasma, electron Langmuir oscillations possesses zero group velocity. Due to this, ray paths of the waves under consideration, being orthogonal to the magnetic field vector, become highly pointed when reflected from the CS.

Orthogonality of group and phase velocities is a characteristic property of potential waves in a cold magnetized

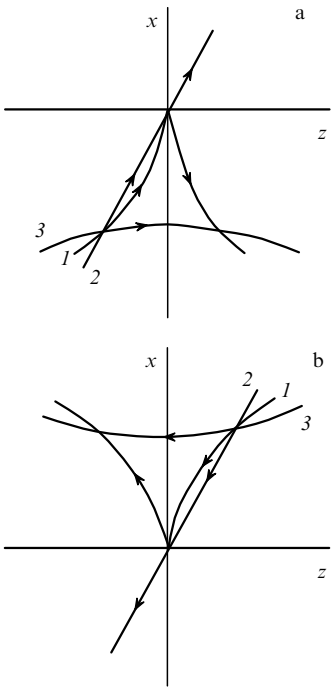

Figure 15. Ray paths of waves incident upon the CS (a) from the lower-density side, and (b) from the higher-density side; *1* — $N_\zeta < N_{\zeta,\sigma}^{\rm opt}$, *2* — $N_\zeta = N_{\zeta,\sigma}^{\rm opt}$, and *3* — $N_\zeta > N_{\zeta,\sigma}^{\rm opt}$.

plasma [see relationship (6.16)]. Waves also become potential in the vicinity of the plasma resonance surface where their refractive index grows ad infinitum. Ray paths in this region were considered by Piliya and Fedorov [30]. It was shown that these paths, like those near the CS, are described by semicubical parabolas. In addition, it should be noted that characteristics of the Euler–Tricomi equation are similarly sharp-pointed at the surface where the gas flow rate comes to exceed the speed of sound (see, for instance, Ref. [31]).

Near the other boundary of the nontransparent region, namely

$$\xi_1 = L\,\delta q_{\rm e,1} = -\frac{2L\sin\chi\,\delta N_\zeta \Omega_{\rm e}^2}{\sqrt{\varepsilon_{\sigma,{\rm c}}}\,g_\sigma(\Omega_{\rm e},\chi)}\,,$$

equation (7.5) yields

$$\zeta \approx {\rm const} \pm \frac{4\Omega_{\rm e}^2}{g_\sigma(\Omega_{\rm e},\chi)\varepsilon_{\sigma,{\rm c}}^{3/4}}\left(\frac{(\xi_1-\xi)\,\delta N_\zeta L}{\sin\chi}\right)^{1/2}. \qquad (7.8)$$

A bundle of ray paths reflected from this boundary gives rise to an ordinary caustic surface (see Fig. 15).

The waves of interest having $N_y = 0$, if $\delta N_\zeta = 0$, completely penetrate through the CS (transmission coefficient equals unity, reflection coefficient is zero). Accordingly, it follows from expressions (7.5) and (7.6) that the ray path looks like a straight line that traverses the CS.

In the case of $\chi = \pi/2$ ($\xi = x, \zeta = z$), expression (7.4) may be used to derive a rather compact equation describing ray paths on both sides of the nontransparent region [12]:

$$z = \pm(2\Omega_{\rm e})^{1/2}\frac{1}{\sqrt{\varepsilon_{+,{\rm c}}}}\left[\sqrt{x(x+x_0)} - {\rm sgn}\,x\,\frac{x_0}{2}\ln\left(\frac{|x+x_0/2|+\sqrt{x(x+x_0)}}{|x_0/2|}\right)\right], \qquad (7.9)$$

where $x_0 = 2L\Omega_{\rm e}\,\delta N_z \varepsilon_{+,{\rm c}}^{-1/2}$. Here, the constant of integration is chosen in such a way that the reflected and incident rays, to which different signs in front of the right-hand side of Eqn (7.9) correspond, coincide at the point of reflection from the nontransparent region, i.e., at $x = 0$ or $x = -x_0$.

For waves that traverse the CS without obstacle, $\mathbf{N} \parallel \mathbf{B}_0$ at the CS itself. When the angle $\chi = \pi/2$, as is typical of closed traps, the wave vector of such waves is orthogonal to ∇n_0. In this situation, the passage of an electromagnetic ray through the CS might appear paradoxical. Indeed, components of the wave vector enter the quantity D (through which the group velocity is expressed) in combinations $N_\perp^2$, $N_\parallel^2$ [see relationships (2.3), (2.4)]. Therefore, at a CS where $N_\perp = 0$, $\mathbf{V}_\perp \propto \partial D/\partial \mathbf{N}_\perp \propto \mathbf{N}_\perp$ should be expected to vanish too. However, it follows from relations (3.7) and (6.10) that the quantity $\partial D/\partial\omega$ at the CS also equals zero. As a result, the transverse constituent of the group velocity remains finite. The vanishing of $\partial D/\partial\omega$ suggests the merging of dependences $\omega(\mathbf{N})$ corresponding to ordinary and extraordinary waves on the critical surface at $N_\parallel^2 = \varepsilon_{\pm,{\rm c}}$ (see Fig. 8). Indeed, in this case it follows from Eqn (2.9) that in the vicinity of the critical surface one finds

$$\omega - \omega_{\rm pe} \approx \pm\frac{|\mathbf{N}_\perp|}{2}\left(\frac{\omega_{\rm e}\omega_{\rm pe}}{2}\right)^{1/2},$$

where the upper sign and the lower sign correspond to ordinary and extraordinary waves, respectively. The latter expression indicates that the transverse component of the group velocity is nonvanishing even at $\mathbf{N}_\perp = 0$.

Complete penetration of microwave radiation through the CS takes place when the equality $N_\zeta = N_{\zeta,\sigma}^{\rm opt}$ strictly obeys. The transmission coefficient obtained from the analysis of the wave equation is a smooth analytical function of the difference $N_\zeta - N_{\zeta,\sigma}^{\rm opt}$. In the case of minor deviations from the optimal value, the coefficient is only slightly different from unity (see Section 6). Ray paths obtained in the approximation of geometric optics behave differently. As shown earlier in this review, any arbitrarily small deflection from a path for wave with $N_\zeta = N_{\zeta,\sigma}^{\rm opt}$ traversing the CS is sufficient to cause oscillations to reflect from this surface ($N_\zeta < N_\zeta^{\rm opt}$) or just before it ($N_\zeta > N_\zeta^{\rm opt}$).

To conclude this section, effects of the thermal electron motion on ray paths need to be considered. Such effects in a nonrelativistic plasma are meaningful only in a narrow region adjacent to the CS, where wave characteristics are similar to those of electron Langmuir oscillations. In this region, thermal effects can be taken into consideration by the redefinition $\varepsilon_\parallel \to \varepsilon_\parallel - 3q_{\rm e}N_\parallel^2\beta_{\rm e}^2$, where $\beta_{\rm e} = (T_{\rm e}/m_{\rm e})^{1/2}/c$.

It is found from condition (2.9) that

$$\omega \approx \omega_{\rm pe} - \frac{\omega_{\rm pe0}\varepsilon_{\perp,{\rm c}}}{2}\,\frac{N_\perp^2(N_\parallel^2-1)}{(N_\parallel^2-\varepsilon_{+,{\rm c}})(N_\parallel^2-\varepsilon_{-,{\rm c}})} + \frac{3\omega_{\rm pe0}}{2}\,N_\parallel^2\beta_{\rm e}^2\,,$$

where $\omega_{\rm pe} \approx \omega_{\rm pe0}(1+\xi/L)$, and $\omega_{\rm pe0} = \omega$. This expression for the frequency indicates that the CS is displaced towards the lower-density side under the influence of thermal electron motion.

The use of the geometrical optics equation (7.1) leads to

$$\begin{aligned}\dot N_x &= A\,,\\ \dot x &= BN_x\,,\\ \dot z &= C_1N_x^2 + C_2\,,\end{aligned} \qquad (7.10)$$

where the following designations are used:

$$A = -\frac{\omega \sin\chi}{L}\,, \qquad B = \frac{(N_\parallel^2 - 1)\omega\varepsilon_{\perp,\mathrm{c}}}{(N_\parallel^2 - \varepsilon_{+,\mathrm{c}})(N_\parallel^2 - \varepsilon_{-,\mathrm{c}})}\,,$$

$$C_1 = \frac{N_\parallel}{(N_\parallel^2 - \varepsilon_{+,\mathrm{c}})^2 (N_\parallel^2 - \varepsilon_{-,\mathrm{c}})^2}\left[(N_\parallel^2 - 1)^2 + \frac{\omega^2}{\omega_\mathrm{e}^2 - \omega^2}\right]\omega\varepsilon_{\perp,\mathrm{c}}\,,$$

$$C_2 = 3\omega N_\parallel \beta_\mathrm{e}^2\,;$$

here, changes in the longitudinal constituent of the refractive index are disregarded, which is relevant at a small distance from the CS.

Equations (7.10) yield

$$N_x = At\,,$$
$$x = \frac{Bt^2}{2}\,,$$
$$z = \frac{C_1 t^3}{3} + C_2 t\,.$$

Ray paths at the XZ surface take the form

$$z = \pm\frac{C_1}{3}\left(\frac{2x}{B}\right)^{3/2} \pm C_2\left(\frac{2x}{B}\right)^{1/2}.$$

At $C_2 = 0$, i.e., in a cold plasma, ray paths are actually semicubical parabolas (see above). Their pointed shape is due to the vanishing group velocity of electron Langmuir oscillations. The group velocity becomes nonzero under the effect of thermal electron motion. As a result, the pointed ray paths are smoothed and, if constants C_1 and C_2 have different signs, the paths make loops in the vicinity of the CS.

8. Wave beams near the critical surface

For the microwave heating of the plasma, electromagnetic waves are fed in the form of wave beams, with the intensity distribution over the cross section being frequently close to a Gaussian one. The penetration of Gaussian wave beams through a CS in the most interesting case of $\chi = \pi/2$ has been considered in Ref. [12].

The ray approximation used in Section 7 is unfit near the wave reflection points (i.e., at the border of the nontransparent region). The corresponding segments of the ray paths in Fig. 15 must be omitted, and the relationship between the ray paths of incident waves and those of transmitted and reflected waves must be found by solving the wave equation. For solving this problem in Ref. [12], ray paths have been considered as the limit of wave packet (wave beam) paths at the ratio of the beam size to the characteristic size of inhomogeneity tending to zero. Certainly, the same approach applies to the ray paths of waves transmitted through the nontransparent region.

Bearing in mind the results of Ref. [12], we shall consider a Gaussian wave beam incident on the CS from the lower-density side ($x < 0$):

$$E(\mathbf{r}) = \int \mathrm{d}N_z\, F(N_z)\, E(\mathbf{r}, N_z)\,, \tag{8.1}$$

where the following designations are used:

$$F(N_z) = \exp\left[-(N_z - N_{z0})^2 l^2\right], \quad E(\mathbf{r}, N_z) = \exp\left[\mathrm{i}\Phi(\mathbf{r}, N_z)\right],$$
$$\Phi(\mathbf{r}, N_z) = \int^x \mathrm{d}x'\, N_x(x', N_z) + yN_y + zN_z\,.$$

The unessential slowly varying pre-exponential factor in the expression for $E(\mathbf{r}, N_z)$ can be discarded.

Far from the critical surface ($|x/x_0| \gg 1$), using the relation (3.6) it can be found that

$$N_x \approx -\frac{x}{\alpha^2} - \frac{A}{2\alpha} + \frac{1}{2x}\left(\frac{A^2}{4} + B_1^2\right); \tag{8.2}$$

hence, one can arrive at

$$\Phi(\mathbf{r}, N_z) \approx -\frac{x^2}{2\alpha^2} - \frac{Ax}{2\alpha} + \frac{1}{2}\left(\frac{A^2}{4} + B_1^2\right)\ln x + yN_y + zN_z + \mathrm{const}\,(N_z)\,, \tag{8.3}$$

where $\alpha = L^{1/2}(\Omega_\mathrm{e}/2)^{1/4}$ and the coefficients

$$A = \frac{2^{5/4}\Omega_\mathrm{e}^{3/4} L^{1/2}\,\delta N_z}{\varepsilon_{+,\mathrm{c}}^{1/2}}\,, \qquad B_1 = \mathrm{Re}\, B = \frac{\Omega_\mathrm{e}^{1/4} L^{1/2} N_y}{2^{1/4}}$$

(see Section 6.1). In the relation (8.2), the sign of N_x has been taken from the condition $V_{\mathrm{gr},x} > 0$. The value of the constant entering Eqn (8.3) may be set equal to $\mathrm{const}\,(N_z) = -(A^2/4 + B_1^2)\ln(-4|x_0|)/2$. Due to this choice, the path of the wave beam whose phase is given by expression (8.3) (see below) coincides with the asymptotics of formula (7.9) for $|x/x_0| \gg 1$. At the same time, this choice facilitates analysis of reflected beam paths.

The spatial dependence of an incident wave beam is found by means of computation of integral (8.1) using the stationary phase method:

$$E(\mathbf{r}) \approx \frac{\sqrt{\pi}}{l_0}\exp\left\{\mathrm{i}\Phi(\mathbf{r}, N_{z0}) - \frac{1}{4l_0^2}\left[\Phi'_{N_{z0}}(\mathbf{r}, N_{z0})\right]^2\right\}, \tag{8.4}$$

where the designations were used:

$$l_0^2 = l^2 - \mathrm{i}A_2 \ln\left|\frac{4x}{x_0}\right|,$$
$$\Phi'_{N_z}(\mathbf{r}, N_z) \approx \frac{1}{2}A_1\left(-\frac{x}{\alpha} + \frac{A}{2}\ln\left|\frac{4x}{x_0}\right|\right) + z\,,$$
$$A_1 = \frac{\partial A}{\partial N_z} = \frac{2^{5/4}}{N_{z0}}\left(\frac{\omega_\mathrm{e}}{\omega}\right)^{3/4} L^{1/2}\,, \qquad A_2 = \frac{1}{8}A_1^2\,.$$

It was assumed in relation (8.4) that $|x/x_0| \gg 1$, and the expression for $\Phi'_{N_z}(\mathbf{r}, N_z)$ is logarithmically accurate in this parameter.

The ray paths considered in Section 7 are naturally associated with the central line of wave beams in which $\Phi'_{N_z}(\mathbf{r}) = 0$. It is easy to see that the wave-beam central line described by expression (8.4) is coincident with the asymptotics of formula (7.9) for $|x/x_0| \gg 1$:

$$z = \frac{A_1}{2}\left(x - \frac{A}{2}\ln\left|\frac{4x}{x_0}\right|\right). \tag{8.5}$$

Simple analytical expressions for a transmitted wave beam can be obtained in two limiting cases: $l \gg L^{1/2}$ (wide wave beam), and $l \ll L^{1/2}$ (narrow wave beam). A wide beam behind the CS is described by expression (8.5) with an additional factor $\exp\left[-\gamma(N_{z0})\right]$ that takes into account efficiency of the tunnel transition. Such a beam is able to completely penetrate through the CS if properly oriented $\left[\gamma(N_{z0}) \ll 1\right]$.

A narrow beam in ordinary space becomes wider in the wavenumber space. The critical surface functions as a filter that cuts out a component with $N_z \approx N_c$ from such a beam. In this case, factor $\exp\left[-\gamma(N_{z0})\right]$ determining the transmission coefficient of the broadened wave beam is replaced by $\exp\left[-(N_{z0} - N_{z,+}^{\rm opt})^2 l^2\right]$. Indeed, saddle-point integration in expression (8.1) gives

$$E(\mathbf{r}) \approx \frac{\sqrt{\pi}}{l_1} \exp\left\{-(N_{z0} - N_{z,+}^{\rm opt})^2 l^2 + i\Phi(\mathbf{r}, N_{z,+}^{\rm opt}) - \frac{1}{4l_1^2}\left[\Phi'_{N_{z,+}^{\rm opt}}(\mathbf{r}, N_{z,+}^{\rm opt})\right]^2\right\}, \quad (8.6)$$

where

$$l_1^2 = \left(\frac{\pi}{4} - i\ln\left|\frac{4x}{x_0}\right|\right) A_2\,, \quad \Phi'_{N_{z,+}^{\rm opt}}(\mathbf{r}, N_{z,+}^{\rm opt}) \approx -\frac{1}{2\alpha}(A_1 x + z)\,.$$

For the effective wave-beam transmission coefficient, it is easy to obtain an expression that, unlike formula (6.1), holds for an arbitrary relationship between l and $L^{1/2}$ [9]:

$$T_b = f^{1/2} \exp\left\{-\pi\left[\frac{fA^2(N_{z0})}{4} + B^2\right]\right\}, \quad (8.7)$$

where $f = l^2/(l^2 + \pi A_2)$. The quantity

$$A_2 = \frac{L}{2^{1/2}(N_{z,+}^{\rm opt})^2}\left(\frac{\omega_e}{\omega}\right)^{3/2}$$

characterizes the width of the radio window for the critical surface in the wavenumber space. Expression (8.7) coincides with formula (6.1) for $l \gg L^{1/2}$, when $f \approx 1$.

It follows from the foregoing that for $l \gg L^{1/2}$ (wide beam), the ray paths of transmitted and incident wave beams are described by one and the same expression (8.5).

Characteristic ray paths for different values of $A \propto \delta N_z$ are displayed in Fig. 16. They are broken at a certain distance from the CS, because the proximity to this surface makes invalid both the quasi-classical approximation and the asymptotic representations (8.3), (8.4), (6.12), and (6.13) that were taken into account to find the spatial dependence of wave beams.

In the case of a narrow wave beam, its component that penetrates beyond the CS travels further along the straight line (8.5) with $A = 0$.

Let us now find the ray paths of reflected wave beams. In order to relate a reflected wave beam to the incident one, expression (6.13), which describes asymptotics of the incident and reflected plane waves, should be used. It was shown above that the path of an incident wave beam is given by Eqn (7.9) at a definite value of the factor entering the first term of expression (6.13) defined accurate to this factor. The same factor must be present in the second term describing the reflected wave. To simplify the computation it is assumed that the condition $\gamma \gg 1$ is met, and the following asymptotic representation is invoked:

$$\Gamma(\gamma) \underset{\gamma \gg 1}{\approx} \exp\left[\gamma \ln(\gamma)\right].$$

With this in mind, the phase of the reflected wave is reduced to expression (8.3) in which the signs of the first three terms are changed to the opposite:

$$\Phi(\mathbf{r}, N_z) \approx \frac{x^2}{2\alpha^2} + \frac{Ax}{2\alpha} - \frac{1}{2}\left(\frac{A^2}{4} + B_1^2\right)\ln\left|\frac{4x}{x_0}\right| + yN_y + zN_z\,.$$

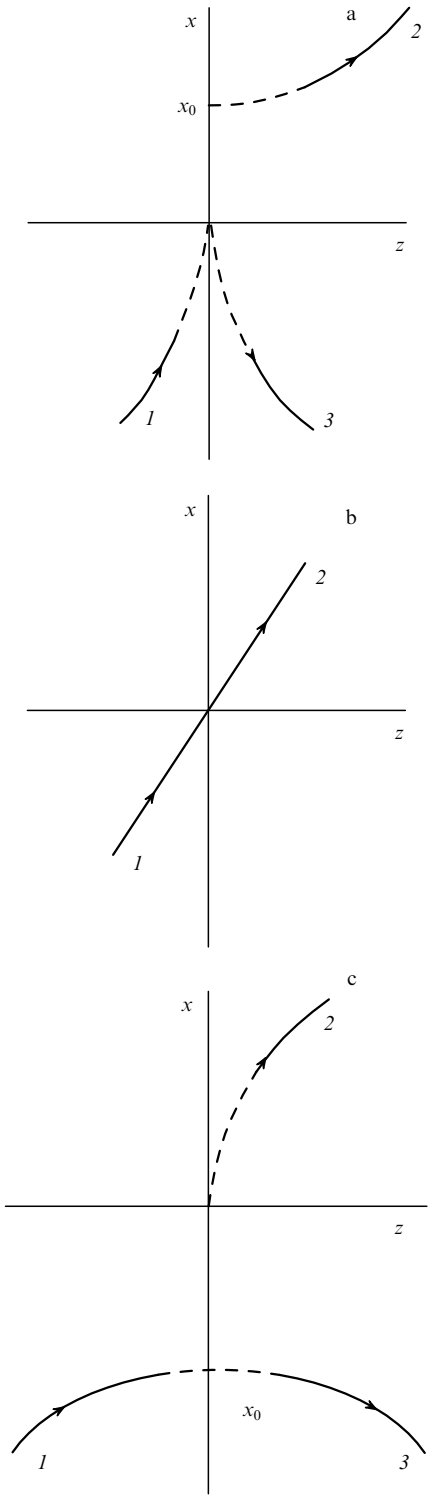

Figure 16. Paths of wave beams incident on the CS from the lower-density side: (a) $N_z < N_{z,+}^{\rm opt}$, (b) $N_z = N_{z,+}^{\rm opt}$, and (c) $N_z > N_{z,+}^{\rm opt}$. The dashed line is a part of the 'path' to which the quasi-classical approximation is inapplicable: *1* — incident beam path, *2* — transmitted beam path, and *3* — reflected beam path.

Using the same procedure to calculate the reflected wave beam, it is found that its path, like that of the incident beam above, coincides with the asymptotics of Eqn (7.9), namely

$$z = -\frac{A_1}{2}\left(\frac{x}{\alpha} - \frac{A}{2}\ln\left|\frac{4x}{x_0}\right|\right).$$

The knowledge of asymptotics allows the entire ray path to be reconstructed. It turns out that the incident and reflected beams are interconvertible at a cusp $x = 0,\ z = 0$ or at the vertex of the 'parabolic' trajectory $(x = -x_0,\ z = 0)$ for $\delta N_z < 0$ and $\delta N_z > 0$, respectively. The merging of the paths is due to taking into account the factor $\Gamma^{-1}(-i\gamma/\pi)$ in the term of Eqn (6.13) that describes the reflected wave. This factor defines the shift of the reflected ray path relative to the incident one as a whole along the Z-axis. Also, its consideration brings the ray path of the transmitted waves closest to the combined ray path of the incident and reflected waves (see Fig. 16).

Upon reflection of a narrow wave beam ($l \leqslant L^{1/2}$) from the CS, it loses part of the Fourier spectrum (region $N_z \approx N_{z,+}^{\rm opt}$). As a result, the reflected beam becomes non-Gaussian and its spatial structure cannot be described by expressions of the form (8.4) or (8.6). The reflected waves broaden up to a size on the order of $L^{1/2}$. Indeed, cutting out a part of the Fourier spectrum of the reflected beam may be interpreted as the formation of another beam having a narrower spectrum, and hence such a beam becomes wider in ordinary space. The phase of the additional reflected beam is π-shifted with respect to the phase of the main beam.

9. Peculiarities of dense plasma microwave heating in magnetic traps

9.1 Open traps

The heating of plasma with microwave radiation is widely employed in current thermonuclear research. At a plasma density above a critical value, there appears a problem for the injected microwaves to penetrate the CS. It was pointed out in Sections 3 and 6 that oscillations pass through the CS without obstacle if their wave vector is parallel to the magnetic field vector. Waves called here left-handed polarized waves (ordinary in the region of $q_e < 1$, and extraordinary in the region $q_e > 1$) emerge at any angle χ between ∇n_0 and $\mathbf{B}_0$. For right-handed polarized waves (extraordinary in the region with $q_e < 1$, and helicons in the region with $q_e > 1$), this angle must be smaller than $\chi_{\max}$ given by the condition (3.4). This accounts for different scenarios of dense plasma heating with microwave radiation in open and closed traps.

Right-handed polarized waves actively interact with the cyclotron electron rotation and their transparent region on the stronger-magnetic-field side extends as far as the cyclotron resonance surface regardless of plasma density. Due to this, right-handed polarized waves can be naturally used for ECR heating by the magnetic beach method. The required configurations of the magnetic field normally apply to open magnetic traps. Angle χ is small ($\chi \ll 1$) near the mirrors, therefore a wave input through them allows the condition $\chi < \chi_{\max}$ to be satisfied.

In closed traps and in the central sections of ambipolar traps, plasma density varies across the magnetic field, when $\chi = \pi/2$. In these cases, only left-handed polarized waves can penetrate the CS, and the O-X-B transformation scheme may be employed for the microwave heating [7] (see Section 6.3).

Let us consider first the heating of a dense plasma in open traps by the magnetic beach method. When the microwave energy is fed through the magnetic mirrors, the optimal ray path is that coincident with the trap axis on which the angle $\chi = 0$. The magnetic beach concept implies that the waves must come to the cyclotron resonance surface from the higher-magnetic-field side. It will be shown below that, in this region, ray paths close to the axis are unstable because refraction due to plasma inhomogeneity results in the exponential enhancement of minor path deviations. In the end, the ray path is repelled towards the rarefied plasma region at the trap periphery.

Let us consider this phenomenon in more details. Plasma density in open traps usually changes more abruptly than a magnetic field. Therefore, a rough assumption of $\mathbf{B}_0(\mathbf{r}) =$ const is relevant and only radial plasma inhomogeneity (a fall with distance from the axis) may be taken into account. Helical waves are described by the approximate dispersion relation (2.13). Assuming the angle between the wave vector and the magnetic field vector to be sufficiently small ($\theta \ll 1$), this dispersion relation may be represented as

$$D = N_z^2(1 - \Omega_e) + N_r^2\left(1 - \frac{\Omega_e}{2}\right) + q_{e0} - r^2 q_{e1} = 0\,. \quad (9.1)$$

Here, the coordinate dependence of plasma density is chosen in the form $n_0(r) = n_0(0) - r^2 n_{01}$, and accordingly $q_e(r) = q_{e0} - r^2 q_{e1}$.

Geometric optics equations (7.2) suggest that the quantity D may be regarded as a Hamiltonian conserved along the ray path. In relation (9.1), the rth component of the refractive index plays the role of momentum, and the quantity $2 - \Omega_e$ the role of 'particle mass'. The effective potential is 'humped' in shape: $U(r) = \text{const} - r^2 q_{e1}$. In the ECR region, $\Omega_e \approx 1$. For this reason, the 'mass' becomes positive as oscillations approach this region. This analogy indicates that minor ray-path deflections from the trap axis must grow.

The above considerations were verified by the computation of ray paths [32] based on the complete dispersion relation (2.3) or (2.4). In these computations, the magnetic field was given by the magnetic potential (see Section 5 for comparison)

$$\Phi(\mathbf{r}) = \Phi_0(z) - \frac{r^2}{4}\,\Phi_0''(z) + \frac{r^4}{64}\,\Phi_0''''(z)\,, \quad (9.2)$$

where

$$\Phi_0(z) = \frac{1}{2}\left[(R+1)z - (R-1)\,\frac{L_B}{\pi}\sin\left(\pi\,\frac{z}{L_B}\right)\right],$$

$$R = 3\,, \qquad L_B = 170\,.$$

The coordinate dependence of plasma density was chosen in the form

$$n_0(\mathbf{r}) = n_0(0)\exp\left[-\left(\frac{r}{L_n}\right)^2\right], \qquad L_n = 65\,.$$

As elsewhere in this review, all quantities with the dimension of length were normalized to c/ω. It was assumed that $\omega_e(0) = \omega$, and $\omega_{pe}^2(0) = 10\omega^2$. These values roughly correspond to the parameters of the open OME trap projected at the Russian Research Centre 'Kurchatov Institute' (Moscow) [34]. It is planned to use this trap for studying stabilization of plasma flute instability with the help of a divertor.

A bundle of 'optimal' ray paths that cross the CS at $N_\perp = 0$ is depicted in Fig. 17. It can be seen that the ray paths go away from the axis, and vectors $\mathbf{N}$ and $\mathbf{V}_{gr}$ turn in the transverse direction as the distance increases.

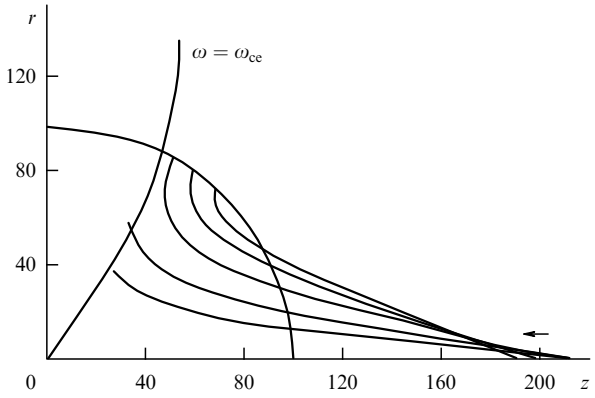

Figure 17. Ray paths of waves with $N_\zeta = N_{\zeta,-}^{opt}$ passing through the CS in an open-trap plasma.

It is widely believed that the waves under consideration (helicons or whistlers) are closely associated with the lines of force of the magnetic field that serve as specific waveguides. This belief is to a certain degree warranted for homogeneous plasmas [4]. However, the analysis has demonstrated that ray paths in an inhomogeneous plasma may significantly deflect from the lines of force of the magnetic field. The negative effect of refraction decreases in the case of flattened radial plasma density profiles.

In thin open traps extended along the magnetic field that changes at distances significantly greater than the plasma cross-sectional dimension, effects responsible for the spreading of wave packets traveling along the ray paths produce radial natural oscillations. The radial distribution of electromagnetic fields and the eigenvalue of the longitudinal wavenumber are adjusted adiabatically according to the parameters of the system (magnetic field, plasma density). In this situation, refraction effects cause waves to contract to the plasma column periphery where the CS is positioned [33].

9.2 Closed traps

Plasma density in closed traps remains constant along the lines of forces of the magnetic field ($\chi = \pi/2$). Only ordinary waves can reach the CS in such systems. A characteristic picture of dispersion dependences for waves with $N_z = N_{z,+}^{opt}$ in a plane plasma layer at $\chi = \pi/2$ is depicted in Fig. 9. It follows from this figure that ordinary waves with $N_z = N_{z,+}^{opt}$ arriving at the CS are transformed into extraordinary ones (O-X transformation). The latter do not penetrate very deeply behind the CS ($\max q_e = 1 + \Omega_e$). When reflected from the dense plasma region, they come up to the plasma (upper hybrid) resonance surface, the position of which is defined by the condition $\omega_{pe}^2 = \omega^2 - \omega_e^2$. In the vicinity of this surface, the extraordinary waves are transformed into potential Bernstein waves (X-B transformation) that penetrate into plasma of arbitrarily high density and are eventually absorbed by it.

Part of a ray path, from the launching point in the vacuum to the plasma resonance surface, can be considered in the cold plasma approximation. However, the description of both the Bernstein waves and the process of their transformation from extraordinary waves requires that effects of the thermal electron motion be fully taken into account. This makes the dispersion relation exceptionally complicated. The relation of interest can be significantly simplified when bearing in mind that the Bernstein waves are potential in character (their refractive index is much larger than unity) and propagate almost transversely to the magnetic field ($\theta \approx \pi/2$). Due to this reasons, for the description of the Bernstein waves it is sufficient to modify the coefficient with the largest (fourth) power of $N_\perp$ in the dispersion relation (2.4) for cold plasma:

$$\varepsilon_\perp \to \varepsilon_B = 1 - \sum_{n=1} \frac{\omega_{pe}^2}{\omega^2 - n^2\omega_e^2} \frac{2n^2}{\xi} I_n(\xi) \exp(-\xi),$$

where $\xi = k_\perp^2 \rho_e^2$, and $\rho_e = \sqrt{T_e/m_e}/\omega_e$. Then, the dispersion relation takes the form

$$D = N_\perp^4 \varepsilon_B + N_\perp^2 \left[N_\parallel^2(\varepsilon_\perp + \varepsilon_\parallel) - 2\varepsilon_\perp\varepsilon_\parallel - \varepsilon_\perp + \varepsilon_\parallel\right] + \varepsilon_\parallel(N_\parallel^2 - \varepsilon_+)(N_\parallel^2 - \varepsilon_-) = 0. \quad (9.3)$$

The effect of ECR absorption of waves with the frequency $\omega \approx \omega_e$ can be included in the consideration by the substitution

$$\frac{1}{\omega - \omega_e} \to -\frac{i\sqrt{\pi}}{k_\parallel v_{Te}} W\left(\frac{\omega - \omega_e}{k_\parallel v_{Te}}\right). \quad (9.4)$$

Here, it is assumed that the argument of the function W is much larger than unity, so that

$$W(\zeta) \approx \frac{i}{\sqrt{\pi}\,\zeta} + \exp(-\zeta^2).$$

Indeed, in the opposite case ($\zeta \leqslant 1$), the imaginary part of W would be comparable to the real one, and the characteristic attenuation length to the wavelength. In this case, it makes no sense to calculate the ray path.

Ray paths for this heating scheme have been computed for a tokamak [35], stellarator [36], and the projected EPSILON closed trap [34]. The last device is a set of open traps linked by curvilinear magnetic field areas. Their magnetic field can be described by the same expression (7.9) that was used earlier. For the purpose of the EPSILON project, the value of $L_B = 440$ in this expression was altered. Also, the last term proportional to r^4 in the expression for the magnetic potential (9.2) was omitted, taking into consideration the longitudinal extension of the system. Unlike isolated open traps, the EPSILON system possesses constant plasma density along the lines of force of the magnetic field, similar to any other closed trap. With this in mind, the plasma density distribution was expressed via the vector potential

$$n_0(\mathbf{r}) = n_0(0) \exp\left(-\frac{rA_\theta}{L_n^2}\right),$$

where

$$A_\theta = \frac{r}{2}\left(\Phi_0' - \frac{r^2}{8}\Phi_0'''\right), \qquad \mathbf{A} = (0, A_\theta, 0), \qquad L_n = 20.$$

Figure 18 shows ray paths in the case when the central density in the trap exceeds the critical one by a factor of 10. It was supposed that $\omega_e/\omega = 0.75$ in the center of the trap. The majority of calculations were carried out on the assumption that $\beta = (v_{Te}/c)^2 = 3 \times 10^{-2}$, i.e., corresponds to a temperature of $T = 7.5$ keV.

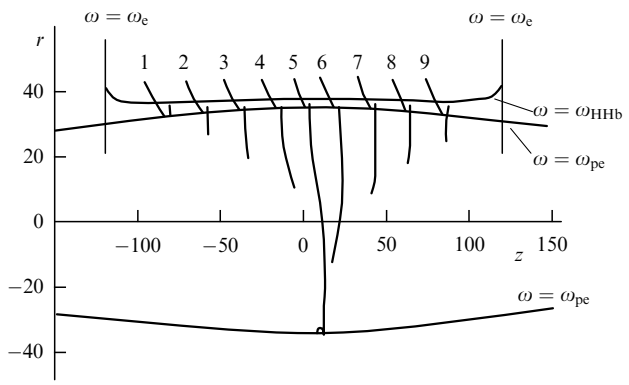

Figure 18. Ray paths of waves with $N_\parallel = N_{\parallel,+}^{\rm opt}$ passing through the CS in the plasma of the projected EPSILON trap.

The ray paths obtained with the use of relation (9.3) are in excellent agreement with the wave propagation pattern described in the preceding paragraphs and illustrated in Fig. 18. Oscillations with $N_\parallel = N_{\parallel,+}^{\rm opt}$ after penetrating the CS are reflected from the dense plasma, then travel outside and traverse the CS again at a unit value of the refractive index (see Section 2). In the vicinity of the upper hybrid (plasma) resonance, extraordinary electromagnetic waves are transformed into potential Bernstein waves with an abrupt rise in the refractive index. The ray paths in the vicinity of the plasma resonance surface are reminiscent of those in the vicinity of the CS. It is small wonder when one bears in mind that in either situation the waves are close to potential ones. The behavior of ray paths near the plasma resonance surface was considered by Piliya and Fedorov [30]. The authors showed that the ray paths of potential waves reflected from the plasma resonance surface form cusps. Precisely such cusps can be seen in the ray paths depicted in Fig. 18 (see also Refs [27, 33 – 36]). In reality, however, ray paths in the vicinity of the reflection point make narrow loops indistinguishable in Fig. 18 because of its small scale. It is conjectured in Ref. [30] that the loops result from wave nonpotentiality.

The Bernstein waves thus formed oscillate between the UHR surfaces until they are fully absorbed. The ray paths shown in Fig. 18 break when their optical thickness amounts to $\tau = 2.5$, where $\tau = \int {\rm d}s\,\varkappa$, $\varkappa$ is the imaginary part of the refractive index, and s is the distance along the ray. An exclusion is ray paths localized near the central plane of the trap. The longitudinal refractive index in such paths is small, therefore they make a large number of radial oscillations prior to being absorbed. In order to avoid filling the central part of the figure with repeatedly intersecting curves, we interrupted each respective ray path after a single radial oscillation.

The absorption strongly (exponentially) depends on the longitudinal refractive index [see Eqn (9.4)]. The growth of plasma density in the ray path leads to the enhancement of the transverse refractive index of the Bernstein wave. The longitudinal component of the refractive index changes thanks to a turn of the wave vector. The longitudinal inhomogeneity of the system is responsible for the refraction. Plasma density in closed traps is constant along the lines of force of the magnetic field, and only the magnetic field changes in the longitudinal direction. In the EPSILON system, the field grows from the median plane (straight line $z = 0$ in Fig. 18) towards the magnetic mirrors. This circumstance and the proximity to the ECR surface account for the enhancement of wave absorption intensity with distance from the median plane. As a result, an input of microwave radiation near the mirrors results in the release of wave energy near the CS. This implies that the waves need to be injected not far from the median plane to ensure heating of the entire plasma column.

The magnetic field in tokamaks varies in the longitudinal direction due to rotational transform, while the quantity $|\mathbf{B}_0 \nabla B_0|$ turns to zero in the equatorial plane and increases with distance from this plane. That is why the waves launched in this plane most deeply penetrate into tokamak plasmas [35].

By virtue of the reversibility of the Maxwell equations, the sequence of wave energy conversions inherent in the B-X-O transformation is made possible in plasma; and this sequence is reverse to that accompanying the O-X-B scheme of plasma heating. Potential Bernstein waves actively interact with the plasma and can be absorbed at distances that are small compared with its extent. At the same time, the plasma may remain transparent for electromagnetic waves of the same frequency. In the latter case, the plasma thermal radiation released through the radio window as a result of the B-X-O transformation is more intense than the radiation directed at different angles. Enhanced plasma emission through the radio window was recorded in Refs [25 – 27].

10. Appendices

Appendix 1

Let us represent the solution to equation (6.25) in the form

$$E_\parallel(\xi) = \int_C {\rm d}p\, \exp(p\xi) f(p)\,. \tag{A1.1}$$

Function $\exp(p\xi)$ must vanish at the ends of the integration contour. This ensures the convergence of integral (A1.1). By substituting (A1.1) into equation (6.25) and integrating by parts, it is found that the function $f(p)$ must satisfy the equation

$$\mathrm{i}\,\frac{4}{L\varepsilon_{\sigma,\rm c}^{1/2}}\,p\,\frac{{\rm d}f}{{\rm d}p} - (-p^2\chi^2 + 2\mathrm{i}\,\delta N_\zeta \chi p + (\delta N_\zeta)^2 + N_y^2) f = 0\,,$$

the solution of which has the form

$$f(p) = p^{-\mathrm{i}\gamma/\pi} \exp\left[\frac{L\varepsilon_{\sigma,\rm c}^{1/2}\chi}{2}\,p\left(\frac{\mathrm{i}p}{4}\,\chi - \delta N_\zeta\right)\right]. \tag{A1.2}$$

Here, $\gamma = \pi L\varepsilon_{\sigma,\rm c}^{1/2}\left[(\delta N_\zeta)^2 + N_y^2\right]/4$ coincides with the limit of Eqn (6.3) for $\chi \ll 1$.

For definiteness sake, we shall consider waves incident on a CS from the lower-density side. Figure 19a shows the integration contour corresponding to the waves escaping from the CS towards the higher-density side. The shaded areas comprise regions where the ends of the integration contour cannot be present because of the (A1.1)-integral divergence. The point $p_{\rm s} = 4\mathrm{i}\xi/(L\varepsilon_{\sigma,\rm c}^{1/2}\chi^2)$ is the saddle point.

The asymptotics of Eqn (A1.1) for $\xi > 0$ is given by the branch point $p = 0$:

$$E_\parallel(\xi) \approx \frac{2\pi\mathrm{i}}{\Gamma(-\mathrm{i}\gamma/\pi)}\,\xi^{-1+\mathrm{i}\gamma/\pi}\,. \tag{A1.3}$$

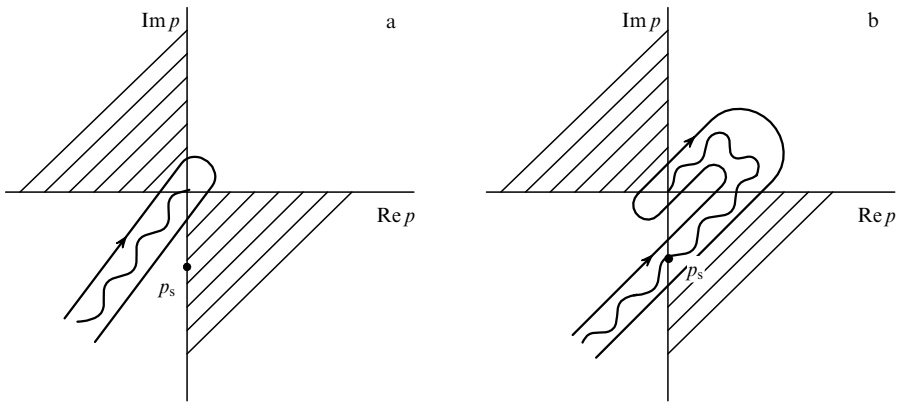

Figure 19. Integration contours corresponding to the waves incident on the CS from the lower-density side: (a) $\xi > 0$, and (b) $\xi < 0$.

Equation (6.25) describes the interaction of circularly polarized and quasi-potential waves. If we were interested in the former waves alone, it would be possible to omit the term with the second derivative in equation (6.25) and supplement the resultant singular first-order equation with the Landau rule of by-passing (see Section 6.2). According to this rule, the singular point

$$\xi_s = \frac{1}{2} L\varepsilon_{\sigma,c}^{1/2}\chi\,\delta N_\zeta$$

must be by-passed in the lower half-plane of the complex variable ξ. The complete equation (6.25) is an analytical one, which makes it possible to change-over to negative values of ξ both via the lower (Landau rule) and the upper half-planes of the complex variable. The first method is simpler because it leads directly to the integration contour shown in Fig. 19b. With the second method, the shape of the integration contour is more complicated because its ends are fixed in the third quarter of the complex variable p. Nevertheless, it can be reduced to the form shown in Fig. 19b. When calculating the contribution of the branching point in this case, as in the former one, it should be assumed that $\arg\xi = -\pi$. Taking into consideration the contribution from both the branching point and the saddle point yields

$$E_\parallel(\xi) \approx \frac{2\pi i}{\Gamma(-i\gamma/\pi)}\,\xi^{-1+i\gamma/\pi} + \frac{2}{\chi}\left(\frac{2\pi i}{L\varepsilon_{\sigma,c}^{1/2}}\right)^{1/2}\left(\frac{4\xi}{L\varepsilon_{\sigma,c}^{1/2}\chi^2}\right)^{-i\gamma/\pi} \times \exp\left(\frac{\gamma}{2}\right)\left[1-\exp(2\gamma)\right]\exp\left(\frac{2i\xi^2}{L\varepsilon_{\sigma,c}^{1/2}\chi^2}\right). \quad \text{(A1.4)}$$

Expression (A1.3) and the first term in formula (A1.4) describe circularly polarized waves. With this in mind, we arrive at the conclusion that their transmission coefficient is given by Eqn (6.1).

The second term in formula (A1.4) corresponds to reflected quasi-potential waves. The coefficient of reflection can be found using expressions for the energy flux. In the case of circularly polarized waves traveling at a small angle to the magnetic field, this coefficient is given by the expression

$$S_\xi \approx \frac{cN_\xi}{4\pi}|E_\sigma|^2, \quad \text{(A1.5)}$$

where

$$E_\sigma \approx \frac{N_\xi N_\sigma}{N_\xi^2 - \varepsilon_{\sigma,c}}\,E_\parallel .$$

It follows from relationship (A1.5) that

$$S_\xi \approx \frac{c}{2\pi}\left(\frac{\xi}{L}\right)^2 \frac{1}{\varepsilon_{\sigma,c}^{3/4}}\,\frac{1}{(\delta N_\zeta)^2 + N_y^2}|E_\parallel|^2 . \quad \text{(A1.6)}$$

It should be noted that $|E_\parallel| \propto |\xi|^{-1}$ [see formula (A1.4) and the first term in formula (A1.5)]; therefore, the energy flux expression is independent of the coordinate.

The following general expression is used for quasi-potential waves:

$$S_\xi = \frac{c}{4\pi}\left(\mathbf{n}_\xi[\mathbf{EB}]\right) \approx \frac{c}{4\pi}(2E_x - \chi E_\parallel)\frac{\partial E_x}{\partial z} .$$

Accounting for asymptotic relations

$$E_x \approx \frac{\varepsilon_{\sigma,c}^{1/2}}{4\delta N_\zeta}\,E_\parallel , \quad \delta N_z \approx \frac{4\xi}{L\varepsilon_{\sigma,c}^{1/2}\chi^2} , \quad N_x \approx \chi\delta N_\xi , \quad N_x \gg N_y$$

yields

$$S_\xi \approx -\frac{c}{64\pi}\,\chi^2|E_\parallel|^2 . \quad \text{(A1.7)}$$

The minus sign in expression (A1.7) corresponds to the picture of wave energy transfer depicted in Figs 8 and 11. The substitution of the first and second terms from formula (A1.4) into expressions (A1.6), (A1.7) gives evidence of the validity of relation (6.2).

Appendix 2

As in Appendix 1, the complex Fourier transform method is used to solve equation (6.26) [see Eqn (A1.1)]. Function $f(p)$ in this expression must satisfy the equation

$$\left\{(p^2+\varepsilon_{+,c})(p^2+\varepsilon_{-,c})\frac{d}{dp} + \varepsilon_{\perp,c}L(p^2+1)\left[(\chi p + iN_\zeta)^2 + N_y^2\right]\right\} f(p) = 0 ,$$

the solution of which has the form

$$f(p) = (p+i\varepsilon_{+,c}^{1/2})^{i\gamma_+^\downarrow/\pi}(p-i\varepsilon_{+,c}^{1/2})^{-i\gamma_+^\uparrow/\pi} \times (p+i\varepsilon_{-,c}^{1/2})^{i\gamma_-^\downarrow/\pi}(p-i\varepsilon_{-,c}^{1/2})^{-i\gamma_-^\uparrow/\pi}\exp(-\varepsilon_{\perp,c}L\chi^2 p) , \quad \text{(A2.1)}$$

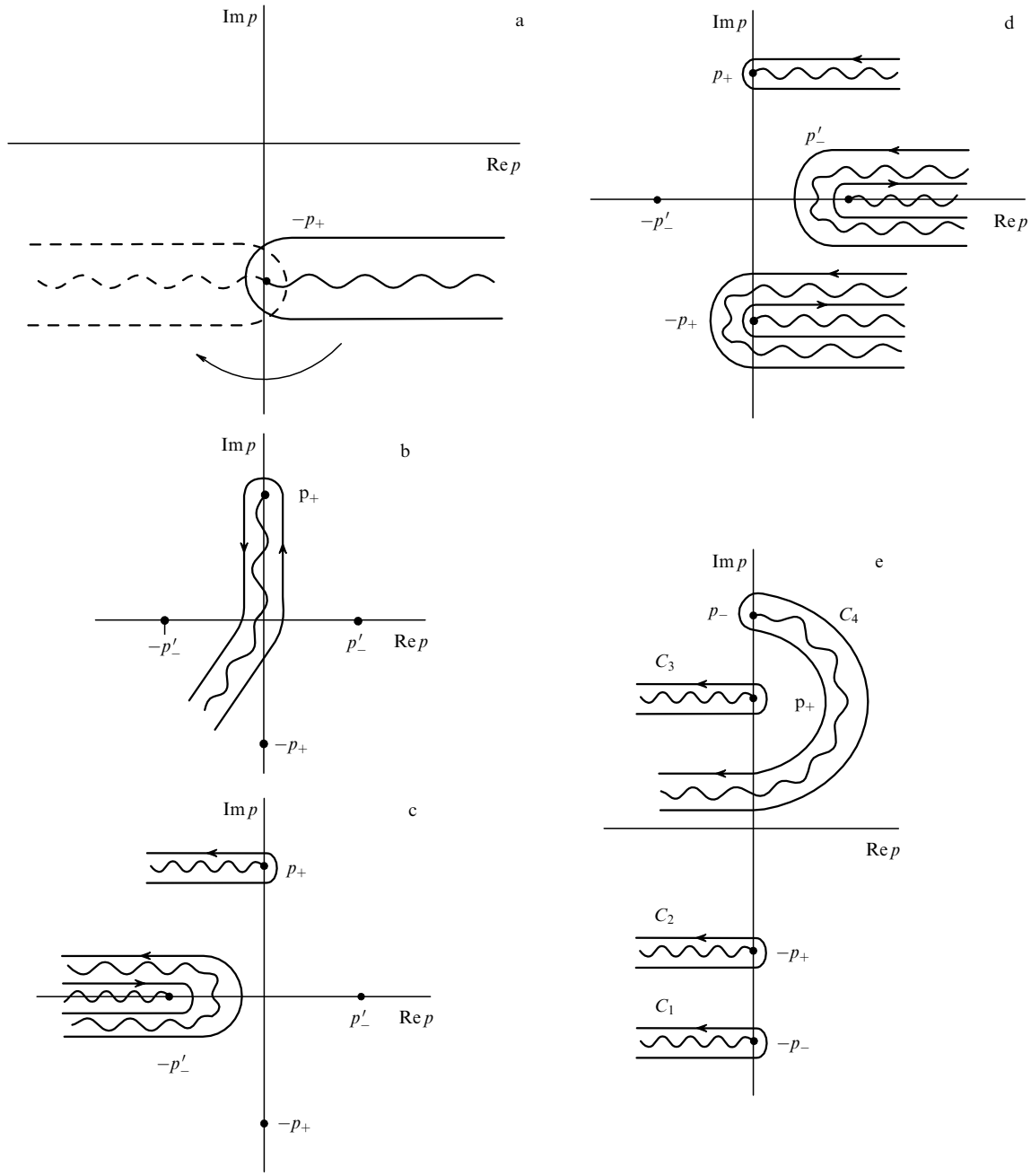

Figure 20. Integration contours in Eqn (A1.1) for the function defined by formula (A2.1); $p_\sigma = \mathrm{i}\varepsilon_{\sigma,\mathrm{c}}^{1/2}$: (a) left-handed polarized wave with $\omega > \omega_\mathrm{e}$ incident upon the CS from the higher-density side, solid line — $\xi < 0$, dashed line — $\xi > 0$; (b) left-handed polarized wave with $\omega > \omega_\mathrm{e}$ incident upon the CS from the lower-density side for $\xi > 0$; (c) deformed contour, other conditions are the same as in figure (b); (d) $\xi < 0$, other conditions are the same as in figures (b) and (c), $p'_- = |\varepsilon_{-,\mathrm{c}}|^{1/2}$; (e) waves with $\omega < \omega_\mathrm{e}$ for $\xi > 0$, C_1, C_2 — right- and left-handed polarized waves, respectively, incident from the higher-density side, C_3, C_4 — right- and left-handed polarized waves, respectively, incident from the lower-density side.

where the following designation is used:

$$\gamma_\sigma^{\uparrow,\downarrow} = \frac{1}{4}\, L\varepsilon_{\sigma,\mathrm{c}}^{1/2}\pi\left[(\chi\varepsilon_{\sigma,\mathrm{c}}^{1/2} \pm N_\zeta)^2 + N_y^2\right],$$

and marks $\uparrow\downarrow$ have the same meaning as in Section 6 — that is, they indicate the direction in which the waves propagate.

Let us consider in greater detail a simpler case of waves with $\omega > \omega_\mathrm{e}$, when only left-handed polarized waves can approach the CS. Let a wave be incident on the CS from the right, i.e., from the higher-density side. Then, the transmitted wave $\propto \exp(-\mathrm{i}\varepsilon_{+,\mathrm{c}}^{1/2}\xi)$ must propagate on the left from the CS. The corresponding integration contour is shown in Fig. 20a. Asymptotics of integral (A1.1) for $|\xi| \gg \varepsilon_{\sigma,\mathrm{c}}^{-1/2}$, $|\varepsilon_{+,\mathrm{c}}^{1/2} - \varepsilon_{-,\mathrm{c}}^{1/2}|^{-1}$ are determined by the small vicinity of the point $p = -\mathrm{i}\varepsilon_{+,\mathrm{c}}^{1/2}$; hence, it is assumed in its computation that

$$f(p) = \mathrm{const}\,(p + \mathrm{i}\varepsilon_{+,\mathrm{c}}^{1/2})^{\mathrm{i}\gamma_+^\downarrow/\pi}. \qquad \text{(A2.2)}$$

This gives

$$E_\parallel(\xi) \approx \mathrm{const}\,\frac{2\pi\mathrm{i}}{\Gamma(-\mathrm{i}\gamma_+^\downarrow/\pi)}\,\xi^{-1-\mathrm{i}\gamma_+^\downarrow/\pi}\exp(-\mathrm{i}\varepsilon_{+,\mathrm{c}}^{1/2}\xi). \qquad \text{(A2.3)}$$

To continue the solution to the region with $\xi > 0$, the Landau rule of by-passing can be used. In conformity with

this rule, such an extension must be effected through the lower half-plane of the variable ξ. In this case, the integration contour must turn clockwise, while remaining in the lower half-plane of the variable p (Fig. 20a). As a result, the same expression (A2.2) in which $\arg(p+\mathrm{i}\varepsilon_{+,\mathrm{c}}^{1/2})$ is reduced by π will be valid for $f(p)$. This means that, in accordance with the results presented in Section 6, the amplitude of the incident wave is $\exp(\gamma_+^{\downarrow})$ times that of the transmitted one, and there are no reflected waves.

The integration contour corresponding to waves incident from the lower-density side is presented in Fig. 20b. It will be shown below that such a choice of $E_\parallel(\xi)$ permits us to avoid in the asymptotics of $E_\parallel(\xi)$ expressions that exponentially grow with distance from the CS. The contour for $\xi > 0$ is convenient to deform as shown in Fig. 20c. Asymptotics of the integral are determined by two branching points $p = \mathrm{i}\varepsilon_{+,\mathrm{c}}^{1/2}$, $|\varepsilon_{-,\mathrm{c}}|^{1/2}$. The contribution from the former yields an expression that describes a wave moving away from the CS, while that of the latter gives an evanescent wave, the amplitude of which falls from the given surface:

$$E_\parallel(\xi) \approx \frac{2\pi\mathrm{i}}{\Gamma(-\mathrm{i}\gamma_+^{\uparrow}/\pi)}\,\xi^{-1-\mathrm{i}\gamma_+^{\uparrow}/\pi}\exp\left(-\frac{\gamma_+^{\downarrow}}{2}\right) \times (2\varepsilon_{+,\mathrm{c}}^{1/2})^{\mathrm{i}\gamma_+^{\uparrow}/\pi}\exp(\mathrm{i}\varepsilon_{+,\mathrm{c}}^{1/2}\xi)C_1 + \frac{2\pi\mathrm{i}}{\Gamma(-\gamma_-^{(1)}/\pi)}\,\xi^{-1-\gamma_-^{(1)}/\pi}\exp\left(-|\varepsilon_{-,\mathrm{c}}|^{1/2}\xi\right)C_2\,,$$

where the following designations are used:

$$C_1 = \left(\mathrm{i}\varepsilon_{+,\mathrm{c}}^{1/2} - |\varepsilon_{-,\mathrm{c}}|^{1/2}\right)^{-\gamma_-^{(1)}/\pi}\left(\mathrm{i}\varepsilon_{+,\mathrm{c}}^{1/2} + |\varepsilon_{-,\mathrm{c}}|^{1/2}\right)^{\gamma_-^{(2)}/\pi},$$

$$\gamma_-^{(1,2)} = \frac{1}{4}\,L\pi|\varepsilon_{-,\mathrm{c}}|^{1/2}\left[\left(\mathrm{i}\chi|\varepsilon_{-,\mathrm{c}}|^{1/2} \mp N_\zeta\right)^2 + N_y^2\right],$$

and C_2 is an unessential constant defining the standing wave amplitude.

Continuation of the solution into the region with $\xi < 0$ results in the integration contours shown in Fig. 20d. Taking into account that, near the point $p = \mathrm{i}\varepsilon_{+,\mathrm{c}}^{1/2}$, the equality $\arg(p - \mathrm{i}\varepsilon_{+,\mathrm{c}}^{1/2}) \approx -\pi/2$ is fulfilled at the inner contour, and the equality $\arg(p - \mathrm{i}\varepsilon_{+,\mathrm{c}}^{1/2}) \approx 3\pi/2$ at the outer one leads to

$$E_\parallel(\xi) \approx \frac{2\pi\mathrm{i}}{\Gamma(-\mathrm{i}\gamma_+^{\uparrow}/\pi)}\,\xi^{-1+\mathrm{i}\gamma_+^{\uparrow}/\pi}\exp\left(-\frac{\gamma_+^{\downarrow}}{2}\right) \times (2\varepsilon_{+,\mathrm{c}}^{1/2})^{\mathrm{i}\gamma_+^{\uparrow}/\pi}\exp(\mathrm{i}\varepsilon_{+,\mathrm{c}}^{1/2}\xi)\,C_1 + \frac{2\pi\mathrm{i}}{\Gamma(-\mathrm{i}\gamma_+^{\downarrow}/\pi)}\,\xi^{-1-\mathrm{i}\gamma_+^{\downarrow}/\pi}\exp\left(-\frac{\gamma_+^{\uparrow}}{2}\right) \times (2\varepsilon_{+,\mathrm{c}}^{1/2})^{\mathrm{i}\gamma_+^{\uparrow}/\pi}\left[\exp(2\gamma_+^{\uparrow}) - 1\right]\exp(-\mathrm{i}\varepsilon_{+,\mathrm{c}}^{1/2}\xi)C_1 + \frac{2\pi\mathrm{i}}{\Gamma(\gamma_-^{(2)}/\pi)}\,\xi^{-1-\mathrm{i}\gamma_-^{(2)}/\pi}\exp\left(-|\varepsilon_{-,\mathrm{c}}|^{1/2}\xi\right)C_3\,.$$

The first two terms in the last expression describe a circularly polarized wave incident upon the CS and reflected from it, while the third term describes a surface wave that exponentially falls off from the surface.

The reflection coefficient can be deduced from the comparison of expressions for energy flows sufficiently far from the CS. Using expression (A1.6) and taking into consideration that, in accordance with Landau's by-passing rule, $\arg\xi = -\pi$ for $\xi < 0$, the coefficients of reflection and transmission are coincident with those presented in Section 6.

The analysis of waves with $\omega < \omega_{\mathrm{e}}$ is analogous to the one applied above and also confirms the results obtained in Section 6. Here, only those integration contours are considered that have been used to find four linearly independent solutions describing circularly polarized waves incident on the CS from both higher- and lower-density sides (Fig. 20e). The peculiar shape of the contour C_4 that describes the incidence of a right-handed polarized wave on the CS from the lower-density side is noteworthy. With such a choice of contour, the region of $\xi < 0$ contains no expressions corresponding to an incident left-handed polarized wave.

References

1. Ginzburg V L *Rasprostranenie Elektromagnitnykh Voln v Plazme* (The Propagation of Electromagnetic Waves in Plasmas) (Moscow: Nauka, 1967) [Translated into English (Oxford: Pergamon Press, 1970)]
2. Zheleznyakov V V *Radioizluchenie Solntsa i Planet* (Radio Emission of the Sun and Planets) (Moscow: Nauka, 1964) [Translated into English (Oxford: Pergamon Press, 1969)]
3. Zheleznyakov V V *Elektromagnitnye Volny v Kosmicheskoĭ Plazme* (Electromagnetic Waves in Cosmic Plasma) (Moscow: Nauka, 1977) [Translated into English: *Radiation in Astrophysical Plasmas* (Dordrecht: Kluwer Acad. Publ., 1996)]
4. Davies K *Ionospheric Radio Waves* (Waltham, Mass.: Blaisdell, 1969) [Translated into Russian (Moscow: Mir, 1973)]
5. Poeverlein H *Z. Phys.* **2** 152 (1950)
6. Ginzburg V *J. Phys. USSR* **7** 289 (1943)
7. Preinhalter J, Kopecky V *J. Plasma Phys.* **10** 1 (1973)
8. Zharov A A *Fiz. Plazmy* **10** 1109 (1984)
9. Mjolhus J *J. Plasma Phys.* **31** 7 (1984)
10. Tokman M D *Fiz. Plazmy* **11** 1205 (1985) [*Sov. J. Plasma Phys.* **11** 689 (1985)]
11. Timofeev A V *Fiz. Plazmy* **26** 874 (2000) [*Plasma Phys. Rep.* **26** 820 (2000)]
12. Timofeev A V *Fiz. Plazmy* **27** 978 (2001) [*Plasma Phys. Rep.* **27** 922 (2001)]
13. Zharov A A, Sergeev M D, Tokman M D *Fiz. Plazmy* **12** 1074 (1986) [*Sov. J. Plasma Phys.* **12** 616 (1986)]
14. Timofeev A V *Fiz. Plazmy* **27** 1046 (2001) [*Plasma Phys. Rep.* **27** 990 (2001)]
15. Timofeev A V *Fiz. Plazmy* **29** 742 (2003) [*Plasma Phys. Rep.* **29** 683 (2003)]
16. Tsytovich V N *Nelineĭnye Effekty v Plazme* (Nonlinear Effects in Plasma) (Moscow: Nauka, 1967) [Translated into English (New York: Plenum Press, 1970)]
17. Timofeev A V *Fiz. Plazmy* **27** 282 (2001) [*Plasma Phys. Rep.* **27** 265 (2001)]
18. Timofeev A V *Rezonansnye Yavleniya v Kolebaniyakh Plazmy* (Resonant Phenomena in Plasma Oscillations) (Moscow: Fizmatlit, 2000)
19. Stix T H *The Theory of Plasma Waves* (New York: McGraw-Hill, 1962) [Translated into Russian (Moscow: Atomizdat, 1965)]
20. Chen F F *Phys. Plasmas* **3** 1783 (1996)
21. Allis W P, Buchsbaum S J, Bers A *Waves in Anisotropic Plasmas* (Cambridge, Mass.: MIT Press, 1963) [Translated into Russian (Moscow: Atomizdat, 1966)]
22. Booker H G *Philos. Trans. R. Soc. London Ser. A* **237** 411 (1939)
23. Melrose D B *Aust. J. Phys.* **33** 121 (1980)
24. Budden K G *J. Atmos. Terr. Phys.* **42** 287 (1980)
25. Laqua H P et al. *Phys. Rev. Lett.* **78** 3467 (1997)
26. Laqua H P, Hartfuß H J, the W7-AS Team *Phys. Rev. Lett.* **81** 2060 (1998)
27. Laqua H P, the W7-AS Team, the ECRH Group *Plasma Phys. Control. Fusion* **41** A273 (1999)
28. Barston E M *Ann. Phys.* (New York) **29** 282 (1964)
29. Abramowitz M, Stegun I A (Eds) *Handbook of Mathematical Functions with Formulas, Graphs, and Mathematical Tables* (New

York: Dover Publ., 1965) [Translated into Russian (Moscow: Nauka, 1979)]
30. Piliya A D, Fedorov V I, in *Vysokochastotnyĭ Nagrev Plazmy: Materialy Vsesoyuz. Soveshch.* (High-Frequency Plasma Heating: Abstr. All-Russia Workshop) (Ed. A G Litvak) (Gor'kiĭ: IPF, 1983) p. 281
31. Landau L D, Lifshitz E M *Gidrodinamika* (Fluid Mechanics) (Moscow: Nauka, 1986) [Translated into English (Oxford: Pergamon Press, 1987)]
32. Timofeev A V *Fiz. Plazmy* **27** 131 (2001) [*Plasma Phys. Rep.* **27** 119 (2001)]
33. Timofeev A V *Fiz. Plazmy* **28** 984 (2002) [*Plasma Phys. Rep.* **28** 906 (2002)]
34. Arsenin V V et al. *Nucl. Fusion* **41** 945 (2001)
35. Smolyakova O B, Tokman M D *Fiz. Plazmy* **26** 833 (2000) [*Plasma Phys. Rep.* **26** 781 (2000)]
36. Nagasaki K, Yanagi N *Plasma Phys. Control. Fusion* **44** 409 (2002)